이학박사 학위논문

The regulation of calcium signal and ion channels in salivary gland

타액선에서 칼슘 신호와 이온 채널의 조절

2021년 8월

서울대학교 대학원

치의생명과학과 치의생명과학 전공

이 지 수

타액선에서 칼슘 신호와 이온 채널의 조절

지도 교수 최 세 영

이 논문을 이학박사 학위논문으로 제출함
2021년 6월

서울대학교 대학원
치의생명과학과 치의생명과학 전공
이 지 수

이지수의 이학박사 학위논문을 인준함
2021년 7월

위 원 장 박 희 경

부위원장 노 상 호

위 원 최 세 영

위 원 박 혜 윤

위 원 정 승 준

Abstract

The regulation of calcium signal and ion channels in salivary gland

Jisoo Lee

Program in Dental Medicine and Life Science
Department of Dental Medicine and Life Science
The Graduate School of Seoul National University

The regulation of saliva secretion is essential for daily life and the main function of the exocrine salivary gland. The salivation is well known to be regulated via muscarinic receptor dependent calcium signaling and flow of chloride ions through the channel as a driving force. In addition, this regulation is responding to the neuronal stimulation, has a similarity to neurons in that it communicates closely with other neurons. Recent studies have suggested that candidate ion channels are related to saliva secretion. However, the expression and function of ion channels on fluid secretion in salivary gland are not well established. This study revealed that calcium (Ca^{2+})-activated ion channels expression and contribution to fluid secretion in salivary gland.

First, certain members of *Anoctamin* (Ano) family have identified that express to secret fluid in salivary gland and contribute to chloride transport by functioning Ca^{2+}-activated chloride channels. Using single-cell RT-PCR technique, the *Ano* isoforms and the major splice-forms in individual acinar or ductal of mouse submandibular gland (SMG) cells were analyzed. Interestingly, *Ano1* was

expressed only acinar cell not ductal cell. In the screen of *Aqp-5* positive cells for the *Ano1* splice variant expression, most cells expressed 'ac' splice form.

Next, the effects of lipid raft microdomains disruption on mouse SMG cells were investigated. Lipid raft microdomains are important for the localization of ion channels in plasma membrane, but it is not well understood whether it affects all membrane events or only specific functions in muscarinic receptor-mediated water secretion in salivary gland cells. It found that incubation with methyl-β-cyclodextrin (MβCD), which depletes lipid raft microdomains, inhibited muscarinic receptor-mediated Ca^{2+} signaling in isolated mouse SMG acinar cells. However, MβCD did not inhibit a Ca^{2+} increase induced by thapsigargin, which activates store-operated Ca^{2+} entry (SOCE). Interestingly, MβCD increased the activity of the large-conductance Ca^{2+}-activated K+ channel (BK channel). Also, MβCD did not directly affect the translocation of AQP5 into the plasma membrane.

Finally, the role of NEGR1 in the salivary glands was studied, which is known to be important for receptor signaling in neurons. Recent transcriptomic studies have revealed that some of the proteins controlling the neuronal functions are also expressed in the salivary glands. However, it is not known how these neuro-exocrine common factors control the physiological functions of the salivary glands. *Negr1* gene was expressed not only in the brain (i.e. cerebral cortex and hippocampus) but also expressed in the salivary glands. The salivary gland morphology of *Negr1* KO mice was the same as normal. In *Negr1* KO mice SMG cells, the carbachol-or thapsigargin-induced intracellular Ca^{2+} increases were decreased. Interestingly in *Negr1* KO mice, the BK channel activity increased. In addition, the surface expression of AQP5 was significantly reduced in *Negr1* KO

mice SMG cells.

These results indicate that multiple anoctamin isoforms are coexpressed in mouse SMG acinar cells, especially *Ano1* 'ac' splice variant, consistent with its involvement in salivary exocrine fluid secretion and potentially, a diversity of splice-form specific roles. And lipid raft microdomains maintain muscarinic Ca^{2+} signaling at the receptor level without directly affecting the activation of SOCE induced by intracellular Ca^{2+} pool depletion or the translocation of AQP5 into the plasma membrane. Also, NEGR1 acts as a regulator of salivation participate in intracellular Ca^{2+} signaling through muscarinic receptors and influences the translocation of AQP5.

Keyword : salivation, ion channels, calcium ion, lipid raft microdomain.

Student Number : 2013-23556

Table of Contents

List of Figures

Chapter 1

Chapter 2

Chapter 3

Abbreviations

GPCR	G-protein coupled receptor
SMG	Submandibular glands
ER	Endoplasmic reticulum
SOCE	Store-operated Ca^{2+} entry
HSG cells	Human salivary gland cells
ANO	Anoctamin, Ca^{2+}-activated chloride channel
BK	Big-K, large-conductance Ca^{2+}-activated potassium channel
AQP5	Aquaporin-5, water transporter
Klk1	Kallikrein-1
MβCD	Methyl-β-cyclodextrin
NEGR1	Neuronal growth regulator 1
PCR	Polymerase chain reaction
WT mice	Wild-type mice
KO mice	Knock-out mice
CCh	Carbachol
Tg	Thapsigargin
ATP	Adenosine triphosphate
IP_3	Inositol 1,4,5-triphosphate
PLC	Phospholipase C

General introduction

1. Salivation

Salivary secretion is a major function of the salivary gland (Pedersen, Sorensen et al. 2018). Salivary glands are divided into major and minor glands by structure and function. Major three salivary glands, which produced 90% saliva of the total, are parotid, submandibular and sublingual glands. The biggest gland is the parotid gland in humans and the submandibular gland in mice (Jensen and Vissink 2014). The functions of saliva are maintenance oral health, buffering, depletion of oral microorganisms, swallowing, taste, digestion (Ngamchuea, Chaisiwamongkhol et al. 2018). It is crucial to regulate the normal level of saliva. Hypofunction of salivary gland induce dry mouth, it has problems of daily life.

1-1. Neuronal regulation

There is neuronal regulation in salivary secretion (Melvin 1999, Bhattarai, Junjappa et al. 2018). Acetylcholine secreted parasympathetic nerve activate muscarinic M1 and M3 receptor and increase intracellular calcium in salivary acinar and ductal cells. Nitric oxide in parasympathetic nerve regulated cAMP-mediated protein secretion in acinar cells. The sympathetic nerve activates β-adrenergic receptor in acinar cells and increases cyclic AMP (Proctor 2016), which is contributed to secret proteins like Amylase. Moreover, salivation is regulated by endocrine and paracrine (Bhattarai, Junjappa et al. 2018). Endocrine disorders like obesity affect salivary function (Modeer, Blomberg et al. 2010). In childhood

obesity, salivary stimulation is decreased. Paracrine neurotransmitter and neuropeptide are related in ion channel and G-protein coupled receptor (GPCR). For example, ATP increases intracellular calcium rapidly in the acinar cell, functions as neurotransmitters. Substance P, as one of the neuropeptides, is localized in the submandibular and parotid gland and induced salivary secretion.

1-2. Calcium signal of salivation mechanism in cells

Salivary gland cells are divided into two groups, acinar and ductal cells, and have cell polarity of apical and basolateral sides. Primary saliva fluid is produced in acinar cells and the fluid is modified through ductal cells (Concepcion and Feske 2017). In primary fluid secretion of the acinar cells, calcium ion is an important signaling molecule (Ambudkar 2014). There were two pathways to increase intracellular calcium. One is calcium release of endoplasmic reticulum (ER), which is the result from GPCR activation. Acetylcholine activates muscarinic receptor in the basolateral membrane, it produces inositol 1,4,5-triphosphate (IP_3) by phospholipase C (PLC). IP_3 binds its receptor in ER, it induces calcium release to cytosol. Another is the influx of extracellular calcium through SOCE (Ambudkar 2016). This store means ER, depletion of ER induced SOCE. SOCE is mediated by a series of factors, including stromal interaction molecule-1 (STIM1), TRPC1 and Orai1 (Ambudkar, de Souza et al. 2017). STIM1-dependent Orai1 and TRPC1 were found to be required for initiating SOCE. STIM1 as an ER Ca^{2+} sensor activates the calcium-selective Orai channels and calcium-permeable non-selective cation TRPC channel to regulate intracellular calcium (Bhattarai, Junjappa et al. 2018). Increase intracellular calcium as a signal activates ion channels (Catalan, Nakamoto et al.

2009). First, it activates Ca^{2+}-activated potassium channel and the cell is hyperpolarized by potassium ions efflux. At the same time, Ca^{2+}-activated chloride channel in the apical cell membrane is activated, induced chloride flow to the lumen is the driving force to fluid secretion. The accumulated chloride concentration in the lumen induced paracellular flow of sodium ion into the lumen, and then this osmotic change of internal and outer cell produced water flow to the lumen paracellularly and through AQP5 water transporter of the apical membrane. The ion concentration of isotonic saliva made in the acinar cells is changed through the process of sodium and chloride reabsorption and bicarbonate and potassium addition in the ductal cells.

2. Ion channels

Ion channels as integral transmembrane proteins diffuse ion molecules across phospholipid bilayers. It has been well known that a key function of ion channels is to mediate the cell interaction with its environment (Becchetti, Munaron et al. 2013). Ion channels transport specific types of ions down their concentration and electric potential gradients. Many channel proteins are usually closed, and opened only in response to specific signals. These types of ion channels play a fundamental role in the functioning of cells. Whereas transporters facilitate the movement of specific small molecules or ions across cell membranes. In contrast to channel proteins, transporters bind one or a few substrate molecules at a time and undergo a conformational change to move molecules across the membrane while maintaining a concentration gradient. Saliva secretion is coordinated by various ion channels (Bhattarai, Junjappa et al. 2018). Saliva is a fluid that contained many ions, the ion

concentration of saliva is different in acinar and ductal cells and is controlled by ion channels (Stummann, Poulsen et al. 2003, Roussa 2011).

2-1. Anoctamin

While chloride ion efflux through Ca^{2+}-activated chloride channels (CaCCs) as a major flow in primary saliva secretion was characterized relatively early, the exact nature of the channel remained a puzzle for a long time (Melvin 1999, Ambudkar 2014). Several proteins (ClC-3, CLCAs, and BESTROPHINs) were proposed as molecular candidates (Duran and Hartzell 2011). But, none of these proteins have properties that exactly fit those of CaCCs. In 2008, studies were reported independently by 3 laboratories that the two genes (*Tmem16A* and *Tmem16B*) have been shown definitively to encode CaCCs (Caputo, Caci et al. 2008, Schroeder, Cheng et al. 2008, Yang, Cho et al. 2008). Tmem16A renamed as Anoctamin1 (Ano1), it means anion move through protein has 8 transmembrane domains (anion+octa=8) (Yang, Cho et al. 2008). This name is now the official and has replaced Tmem16 in Genbank. *Ano1* is one of the superfamily that has 10 genes (Berg, Yang et al. 2012). The functions of anoctamins are involved in ion transport, phospholipid scrambling, and regulation of membrane proteins (Pedemonte and Galietta 2014, Benarroch 2017). Only ANO1 and ANO2 revealed CaCC function, the function of other anoctamin family members as channels is unclear. *Ano1* knock-down mice showed greatly decreased CaCC and salivary production (Yang, Cho et al. 2008). In addition, reduced salivation was reported in *Ano1* acinar cell-specific conditional knockout mice (Catalan, Kondo et al. 2015). It suggesting that ANO1 is involved in primary saliva secretion.

2-2. BK channel

Calcium-activated potassium ion channels have been certified their key functions are associated with membrane potential regulation, potassium ion movement and fluid secretion in exocrine glands (Catalan, Nakamoto et al. 2009). Two different potassium channels have been identified in exocrine salivary glands, one of which is a Ca^{2+}-activated potassium channel of intermediate single channel conductance encoded by the *Kcnn4* gene, and is named IK1 or SK4. Another potassium channel is a voltage- and Ca^{2+}-dependent potassium channel of large single channel conductance encoded by the *Kcnma1* gene, and is named BK or maxi-K. Salivary gland fluid secretion was severely impaired in mice lacking both IK1 and BK channels (Romanenko, Nakamoto et al. 2007). Surprisingly, potassium ion secretion was inhibited >75% in mice lacking *Kcnma1* gene but was unchanged in mice with a mutation in the IK1 channel (Nakamoto, Romanenko et al. 2008). Further, paxilline as a specific BK channel inhibitor decreased the potassium ion concentration in SMG saliva. The potassium ion concentration of saliva is well proved to be flow rate dependent, the flow rate dependence of potassium ion secretion was impaired in *Kcnma1* null mice. These results indicated that a critical role for BK channels in salivation.

BK channel activity in the acinar cells is a critical Ca^{2+} dependent process required for fluid secretion. BK channels located at the basolateral membrane of acinar cells are necessary to mediate potassium ion efflux and hyperpolarize the cell membrane, thus increasing the driving force for chloride ion efflux to the lumen.

3. Lipid raft microdomain

Lipid rafts are defined as nanodomains within the membrane lipid bilayer, that are enriched with cholesterol, sphingolipids and gangliosides (Gueguinou, Gambade et al. 2015). The role of lipid raft microdomain is to promote signaling (Allen, Halverson-Tamboli et al. 2007). The signaling molecules were organized location by lipid raft microdomain. It is well known that lipid rafts are important for the trafficking and signaling of GPCRs (Villar, Cuevas et al. 2016). Lipid rafts as dynamic platforms for GPCRs organize pertinent signaling molecules such as adaptors proteins and enzymes. In addition, many ion channels are found to be expressed in lipid rafts. They organize ion channels and their downstream molecules to promote intracellular signaling pathways. Lipid raft microdomains serve as a signaling platform for the organization and dynamic interaction involved in neurotransmitter signaling (Allen, Halverson-Tamboli et al. 2007), endocytosis, and protein trafficking. Furthermore, the lipid composition of rafts is dramatically altered in cancer (Gueguinou, Gambade et al. 2015). It is well known that BK channel is located in lipid raft microdomain. However, the disorder of the lipid raft by cholesterol depletion induced abnormal BK activity. The effect of BK channel is different by cell type (Weaver, Olsen et al. 2007, Bukiya, Vaithianathan et al. 2011, Tajima, Itokazu et al. 2011). However, in the salivary gland, disruption of the lipid raft to affect BK channel activity is not known. Therefore, the specific localization and regulation of GPCR and BK channels in lipid raft microdomains need to be addressed in salivary gland cells.

4. Purpose of this study

Regulation of salvation is critical in oral health, it requires the coordinated activity of multiple ion channels and receptors. Recent studies revealed that a better understanding of the saliva secretion process, due to molecular cloning and gene knock-out technique of many proteins involved in fluid secretion. However, their exact contribution of calcium signal and ion channels to salivary secretion has not been directly demonstrated.

The main purpose of this study is to investigate the molecular mechanisms in salivation. To achieve this goal, the spectrum of anoctamin isoform expression in single acinar or ductal cells of mouse SMG was examined using single-cell RT-PCR technique. Next, it was elucidated that the involvement of lipid raft microdomain in mouse SMG cells. Finally, it suggested a regulate factor protein involved in salivation to control Ca^{2+} signal and diverse ion channel components.

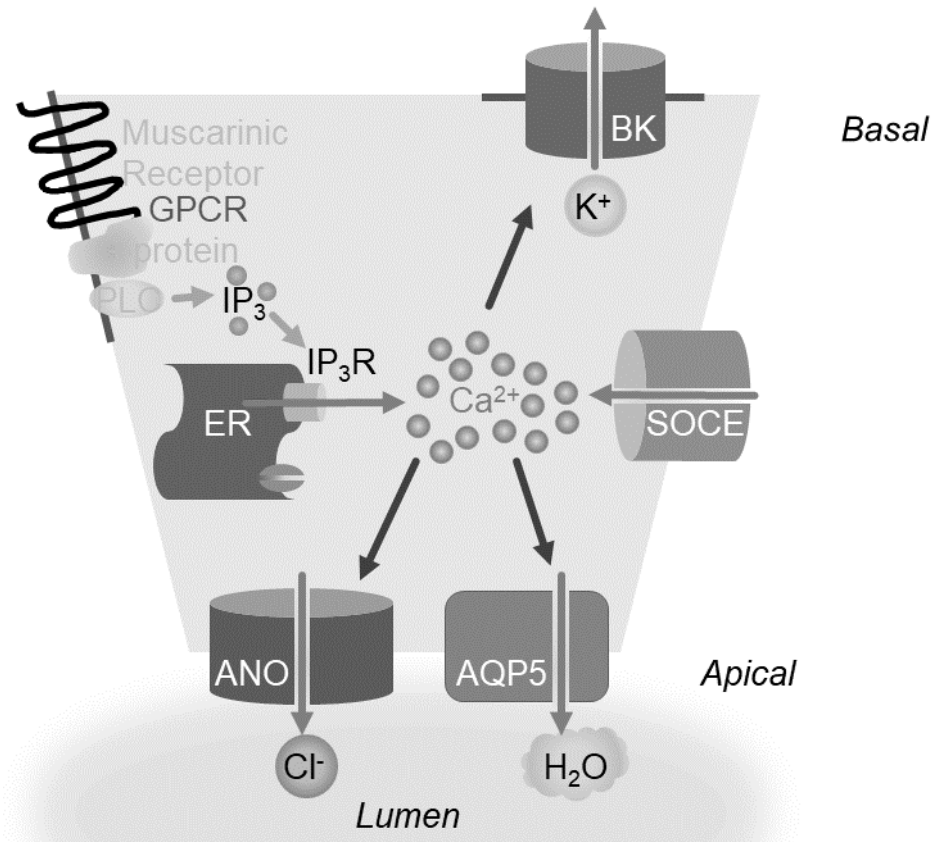

Calcium signal and ion channels of salivation mechanism in salivary acinar cell.

Chapter 1.

Ca^{2+}-activated chloride channels expression in mouse submandibular gland (SMG) cells

Introduction

Chloride ions transport into the lumen of salivary acinus is rate-limiting in salivary exocrine fluid secretion. Several channels have been reported as a candidate for the calcium-activated chloride channel in the salivary gland: ligand-gated anion channels, CFTR, CICs, BESTROPHINs, and ANOCTAMINs (Duran and Hartzell 2011, Bhattarai, Junjappa et al. 2018). BESTROPHINs and CFTR are chloride channels and transporter, respectively. Members of ANO family of proteins function as CaCCs that likely mediates this chloride flux in mouse salivary acinar cells (Yang, Cho et al. 2008). It was proved that Ca^{2+}-dependent salivation was decreased greatly in acinar cell-specific *Ano1* conditional knockout mice (Catalan, Kondo et al. 2015). The ANO family includes 10 members (ANO1 to ANO10), with distinct distributions in tissues (Benarroch 2017). They are highly conserved intracellular calcium–activated proteins with multiple cellular functions. Except for ANO1 and ANO2, the function of other anoctamins is unclear (Berg, Yang et al. 2012).

A recent study revealed that mRNAs for multiple *Anoctamin* isoforms were expressed in mouse salivary glands (Han, Kim et al. 2015), not only *Ano1* but also *Ano6, Ano10* existed in mouse SMG. Furthermore, it has been identified 4 splice variants for *Ano1*, the variant with all 4 segments is designated as *Ano1*-abcd (Ferrera, Caputo et al. 2009). ‘a’ and ‘b’ segments are located in the N-terminus and ‘c’ and ‘d’ segments are in the first intracellular loop. The 4 splice variants of ANO1 have different voltage-dependent and Ca^{2+}-dependent gating activity (Strege, Gibbons et al. 2017). For example, *Ano1* with ‘c’ segment was changed chloride currents at low intracellular calcium concentration.

To better identify the role of anoctamin proteins in salivary gland function, it is pivotal to demonstrate which of the anoctamin isoforms is present in the tissue. Using the single-cell RT-PCR technique, it analyzed the anoctamin isoforms and the major splice-forms in individual acinar or ductal cells of mouse SMG.

Materials and Methods

SMG single-cell preparation

SMGs freshly isolated from 12 weeks old C57BL/6 male mouse. SMGs were finely minced in phosphate buffered saline (PBS) supplemented with 10 mM sodium pyruvate (Bionics, Korea), a 0.02% trypsin inhibitor (Bionics, Korea), and 0.1% bovine serum albumin (BSA, Gibco, USA) for 10 min on ice. The cells are transferred in 50 mL Glass Spinner Flask with Double Sidearms (Wheaton, USA) and digested in the same solution containing 0.05 mg/ml collagenase P (0.04 mg/ml, Roche, Switzerland) at 37℃ for 30 min with oxygen and continuous gentle stirring. The cells were dispersed by trituration through a heat-polished pasteur pipette 10 times every 10 min using decreasing pore sizes (L-M-S). The cell was collected in a 50 ml conical tube (196x *g* for 50 sec) and washed twice with PBS or serum-free DMEM media. The resuspended cells in serum-free media are filtered through 70 μm cell strainer (BD falcon, USA). 2~4 drops of cells are seeded onto Poly-D-Lysine (Cultrex, USA)-coated 35 mm dish for single-cell picking.

Single-cell pick and cDNA synthesis

The majority of cells were typically picked after overnight incubation at 37℃. The dish is washed twice with Diethylpyrocarbonate (DEPC)-PBS and single cells are picked using patch clamping technique. A picked single cell is collected in a PCR tube with 7.2 μL RT Mix1 solution on ice. RT Mix1 solution is contained DEPC-water, Rnase inhibitor (20 units, Enzynomics, Korea) and the specific reverse primers mixture (10 pmole each). These PCR tubes containing single cell are stored at -70°C freezer. When complementary DNA (cDNA) synthesis reaction, the frozen

cells in PCR tubes are vortex and spin down and 70℃ incubation for 5 min. Then the tubes are transferred on ice and added 4.8 μL RT Mix2 solution. The RT Mix2 solution is contained M-MLV reverse transcriptase (200 units, Promega, USA), 50 mM Tris-HCl (pH 8.3), 75 mM KCl, 3 mM $MgCl_2$, 10 mM dithiothreitol, 25 mM dNTPs and RNase inhibitor (40 units, Enzynomics, Korea). After the solution in PCR tubes is mixed and spin down, the cDNA synthesis cycle goes on 42℃ for 1 hr, 70℃ for 10 min. The cDNA was stored at -20℃ until use.

Polymerase chain reaction (PCR)

PCR was performed using Ex Taq polymerase (0.5 Units, Takara, Japan), 1 μl of cDNA template from RT reaction, forward and reverse primers each at 0.8 μM, dNTP each at 4 mM in 20 μl reaction. The protocol consisted of incubation at 95℃ for 2 min followed by 40-45 cycles of 95℃ for 10 sec, 54.5℃ for 10 sec, 72℃ for 35 sec and extended at 72℃ for 5 min in Biorad thermocycler (USA). All of the amplified reaction was electrophoresed on a 1.5% agarose gel. Information of specific PCR primers designed as shown in Table1.

Table 1: Oligonucleotide primers used in single cell RT-PCR

Target	F /R	Primer sequence 5'-3'	product length (bp)
Aquaporin-5	F	CCATTCTGCAGATCTCCATAG	390
	R	GTGTGACCGACAAGCCAATG	
Kallikrein-1	F	ACCCAGATGAGCTCCAGTGT	219
	R	GCACATTGGGTTTACCGCAA	
Anoctamin1	F	GCCAGAGTCTTAGAGAAGTCACTG	481
	R	AAGAGCGGAAGATGTACACGTAG	
Anoctamin6	F	CTCCTCATGCTTCTACATCG	285
	R	ATGGGCTGCAGATGGTAATC	
Anoctamin10	F	GATTGAGATCATGAACCGCCTCT	395
	R	CACATAGCCAAACTGCAGGAAC	
Ano1 b form (Primer b +)	F	CAGGCCACAGACCACAAAGA	230
	R	ACCGTATTTCCCACACTTCCG	
Ano1 b form (Primer b -)	F	CAGGCCACAGACCACAAAGA	177
	R	AGGCTGGTGATACCCATGC	
Ano1 c, d form (Primer c +)	F	GAAGCTGTCAAGGATCATCC	200 or 270 (d -)
	R	GATGATAACTCCGAGGACGAT	
Ano1 c, d form (Primer c -)	F	CGAGGAGGAGGAGGATCAT	271 or 199 (d -)
	R	GATGATAACTCCGAGGACGAT	

Result

Differences of *Ano1* or *Ano6*, or *Ano10* expression in acinar and ductal cells

Anoctamin 1, 6, and *10* isoforms are abundant in mouse SMG. Single-cell PCR technique resulted in the overall success rate of 73.5% (n=260). Approximately, 60% of acinar cells expressed one of *Ano1*, *Ano6* and *Ano10*, compared to ductal cells that expressed no *Ano1*, and lower percentages of *Ano6* (22%) and *Ano10* (20%). Cells that did not amplify acinar cell marker (*Aqp5*) or ductal cell marker (*Klk1*) was 11%. The false-positive rate was assumed to be 0% for *Ano1*, 8% for *Ano6*, and 1% for *Ano10*. There are differences in *Ano* transcript expression in acinar and ductal cell types. In acinar cells, there were approximately 60% of cells expressing *Ano1* or *Ano6*, or *Ano10*, and approximately 40% of cells that did not express any *Ano* transcripts. The proportion of cells expressing *Ano* transcripts were reversed in ductal cells. *Ano1* expression and its combination with *Ano6* and *Ano10* transcripts occurred more frequently in acinar cells. Only individual or combinations of *Ano6* and *Ano10* transcripts were expressed in ductal marker positive cells. Both *Ano6* and *Ano10* transcripts expression correlated with ductal marker expression and *Ano1* expression correlated with acinar marker expression.

Single-cell splice variant form analysis of *Ano1* in SMG acinar cell

In a 48-cell screen of *Aqp5* positive cells for the *Ano1* splice variant expression, there were 37 cells were positive for *Ano1* expression and 11 cells were negative. Among *Ano1* expressing cells, 17 cells expressed ‘ac’ form of *Ano1*, 2 cells expressed ‘abc’ variant form, there were no cells with *Ano1* that included ‘d’ splice variant, and 18 cells in which the ‘b’ or ‘c’ splice forms were uncertain. Most of

Ano1 splice forms in SMG acinar cells are the variant lacking segments ‘b’ and ‘d’.

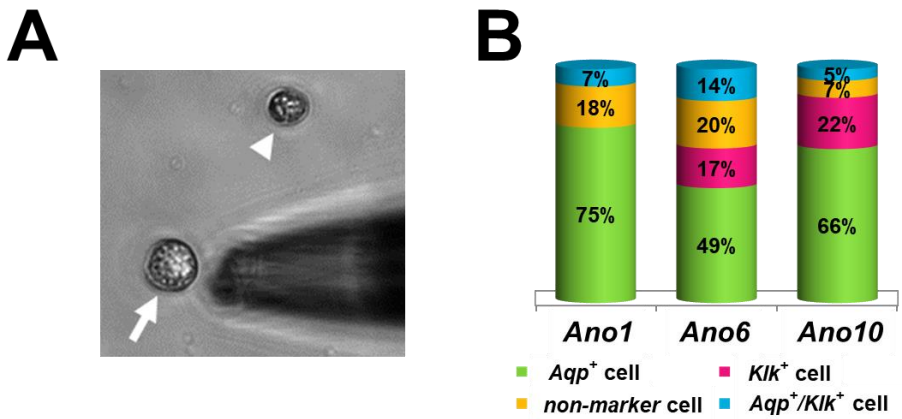
A
B
7%
18%
75%
14%
20%
17%
49%
5%
7%
22%
66%
Ano1
Ano6
Ano10
Aqp+ cell
Klk+ cell
non-marker cell
Aqp+/Klk+ cell
C
no Cell Con
Cell 1 ~ 7
M
Cell 9 ~ 13
no Cell Con
PCR neg. Con
1
2
3
4
5
6
7
8
9
10
11
12
13
14
15
16
Aqp5
Klk1
Ano1
Ano6
Ano10

Figure 1-1. *Anoctamins* transcripts expression in mouse SMG acinar and ductal single cells

A. Capture figure of primary single-cell collection using pulled glass pipettes under a microscope. Arrow indicated acinar cell and arrowhead indicated ductal cell.

B. Differences in the proportion of acinar and ductal marker expression in *Ano1* or *Ano6*, or *Ano10* expressing cells. Seventy-five percent of *Ano1* expressing cells were also positive for *Aqp5*$^{+}$. There were no ductal marker (*Klk*1^{+}) positive cells among *Ano1* expressing cells. There were 66% of *Ano10* positive cells and 49% of *Ano6* positive cells were acinar marker positive.

C. Representative gel images of single-cell RT-PCR assay. *Aqp5* primer set was used as acinar cell marker and *Klk1* primer set was used as a ductal cell marker. Samples of individual single-cell RT reactions were used to amplify *Aqp5*, *Klk1*, *Ano1*, *Ano6*, *Ano10* in separate PCRs. no Cell Con; negative control as the solution without cell, M; The marker of PCR product size, PCR neg. Con; no cDNA template as a negative control of PCR assay.

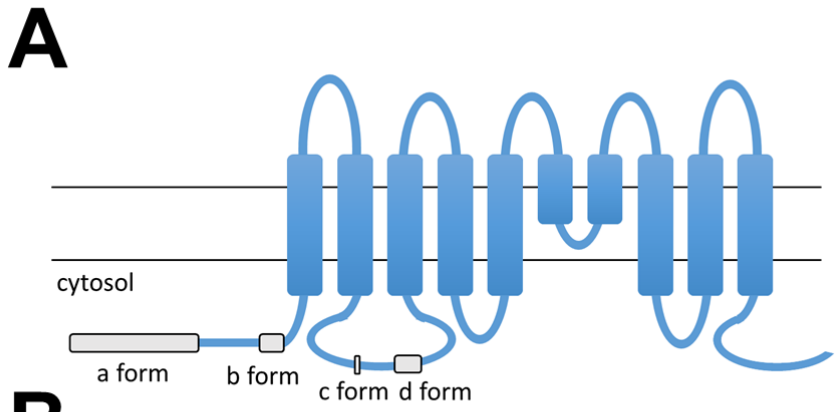
A
cytosol
a form
b form
c form
d form

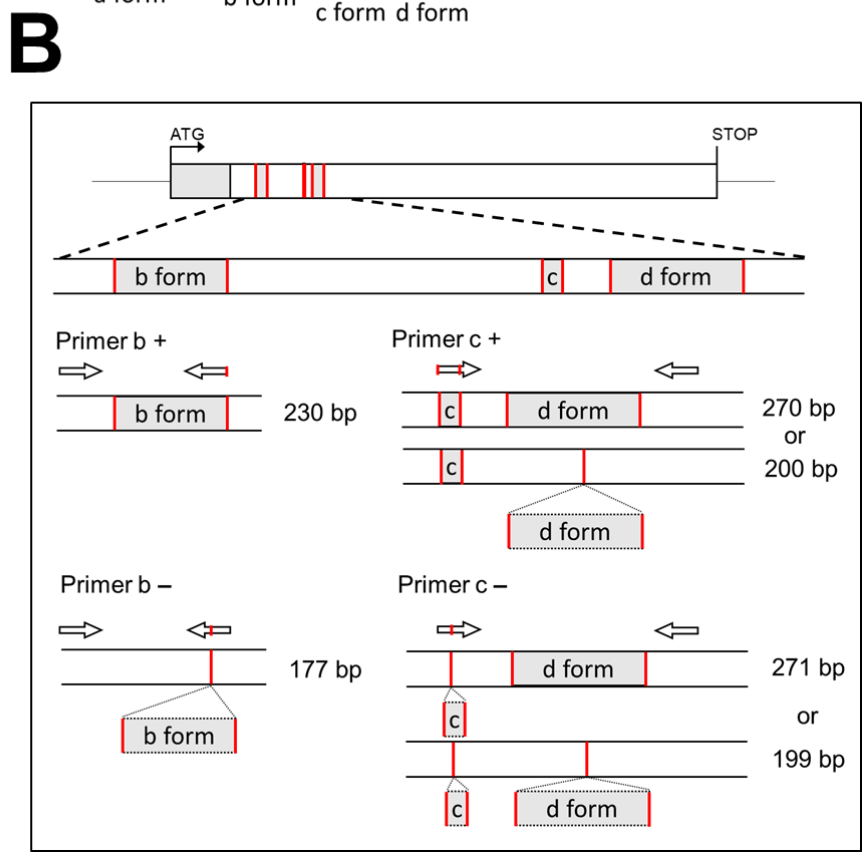
B
ATG
STOP
b form
c
d form
Primer b +
b form
230 bp
Primer c +
c
d form
270 bp
or
c
200 bp
d form
Primer b –
177 bp
b form
Primer c –
d form
271 bp
or
c
199 bp
c
d form

Figure 1-2. Primer design for identifying splice variant form of *Ano1*

A. Predicted ANO1 membrane topology and splicing sites. The schematic diagram modified from Ferrea and colleagues' report (Ferrera, Caputo et al. 2010). 8 putative transmembrane domains with a reentrant loop between the fifth and the sixth domain. The diagram also shows the position and comparative size of the four alternative segments: a, b, c, and d.

B. Specific primer sets were designed for identifying splice variant forms of *Ano1*. To detect splice 'b' form, two primer sets were designed and forward primer was used commonly. If 'b' form exists, only PCR product amplified in the tube containing 'Primer b +' set. Conversely, if there is no 'b' form, the band will appear only in 'Primer b -' set. To identify 'c' and 'd' forms, two primers set were designed and the reverse primer was used commonly. If 'c' form exists, only PCR product amplified in the tube containing 'Primer c +' set and existence of 'd' form is determined by product size. Conversely, if there is no 'c' form, the band will appear only in 'Primer c -' set and the existence of 'd' form is determined by product size.

A

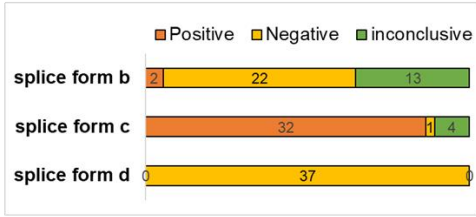
Positive
Negative
inconclusive
splice form b
2
22
13
splice form c
32
1
4
splice form d
0
37
0

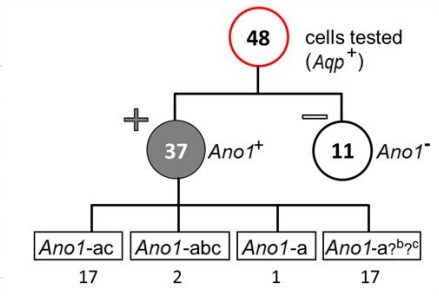
48
cells tested
(Aqp+)
+
37
Ano1+
−
11
Ano1-
Ano1-ac
17
Ano1-abc
2
Ano1-a
1
Ano1-a?b?c
17

B

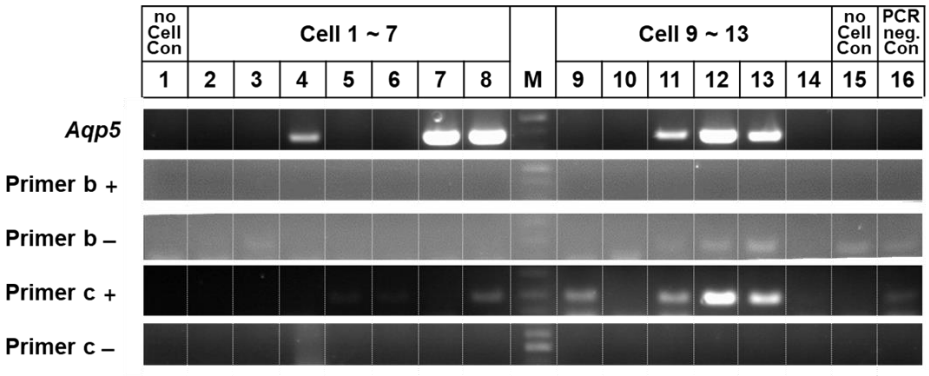
no Cell Con
Cell 1 ~ 7
M
Cell 9 ~ 13
no Cell Con
PCR neg. Con
1
2
3
4
5
6
7
8
9
10
11
12
13
14
15
16
Aqp5
Primer b +
Primer b –
Primer c +
Primer c –

Figure 1-3. Splice variant (b, c, d form) of *Ano1* in SMG acinar cell

A. Bar graph and hierarchy diagram of results. Numbers indicate counted cells. (Left) The number of positive and negative cells represented by each splice variant. (Right) '+' indicated positive expression and '-' indicated negative expression. The majority of *Ano1* splice variants of the acinar cells are 'ac' forms.

B. Representative gel images of single-cell RT-PCR assay. *Aqp5* primer set was used as an acinar cell marker. To discriminate the expression of a,b,c and d splice forms of *Ano1*, four primer sets were used. Aliquots of cDNAs were used in individual PCR reactions to amplify each gene product. no Cell Con; negative control as the solution without cell, M; The marker of PCR product size, PCR neg. Con; no cDNA template as a negative control of PCR assay.

Discussion

The key to the formation of primary saliva in the acinar cells is the movement of the chloride ion. The efflux of chloride ion to the lumen is through a certain channel, it activated intracellular calcium signal. CaCCs have important roles in trans-epithelial ion transport, smooth muscle contraction, and control of neuronal excitation (Pedemonte and Galietta 2014). Only ANO1 and ANO2 have known roles as CaCCs, other anoctamins are associated with ion transport, phospholipid scrambling, and regulation of membrane proteins (Pedemonte and Galietta 2014).

In this study, the expression of *Ano1*, *Ano6*, and *Ano10*, which are known to be expressed in mouse SMG, was confirmed by distinguishing acinar and ductal cells. Single-cell RT-PCR technique is used to study the molecular identities and mechanistic details of mRNA involved in individual cells of salivary gland. Interestingly, it was proved that *Ano6* and *Ano10* were expressed more in acinar cells than in ductal cells. These results suggest that multiple anoctamin isoforms are co-expressed within single mouse submandibular salivary gland cells. In addition, *Ano1* expression appears restricted to acinar cells, especially *Ano1* 'ac' splice variant, consistent with its involvement in salivary exocrine fluid secretion and potentially, a diversity of splice-form specific roles.

It was demonstrated that it modulates voltage and calcium dependence of CaCCs, according to the splice variant of ANO1 (Ferrera, Caputo et al. 2009). Especially, it was certified that 'c' segment of ANO1 reduces the calcium sensitivity of channel activation and deactivation by slowing activation kinetics (Strege, Gibbons et al. 2017). Moreover, depending on the ANO1 splice variant, the degree of inhibition for the same blocker is different (Sung, O'Driscoll et al. 2016).

The type of anoctamin expressed in SMG, especially acinar cells, and the correct splice variant were identified. Through these results, it is expected that ANO1 will be used as an acinar cell marker. Also, knowing the exact structure of ANO1 expressed in SMG will help develop target drugs.

Chapter 2.

The Effect of Ca^{2+} signal and Ca^{2+}-activated potassium channels on lipid raft microdomains in mouse SMG cells

This chapter has been largely reproduced from an article published by Lee, J., Kim, Y.-J., Choi, L.-M., Lee, K., Park, H.-K., and Choi, S.-Y. (2021) International Journal of Molecular Science, 22(9).

Introduction

Exocrine gland cells use GPCRs to accept extracellular signals and regulate several cellular activities. For example, in the salivary gland, Ca^{2+} signaling of GPCRs induces membrane translocation of AQP5 (Tada, Sawa et al. 1999, Delporte 2014). The GPCR activation and subsequent translocation of aquaporin require well-organized signaling pathways that function based on environmental cues. The lipid raft microdomain is cell membrane microdomains composed of cholesterol, glycolipids, sphingolipids, and specific proteins that acts as the main center of signal transmission (Sebastiao, Colino-Oliveira et al. 2013, Aureli, Grassi et al. 2015). Lipid raft microdomains play an important role in various cellular processes, such as signal transduction, protein trafficking, exocytosis, endocytosis, chemotaxis, and cell migration (Simons and Sampaio 2011). Particularly in cells with apical-basolateral polarity, lipid raft microdomains have a significant impact on physiological functions. These lipid raft microdomains also contain receptors and ion channels (Allen, Halverson-Tamboli et al. 2007, Sebastiao, Colino-Oliveira et al. 2013). Therefore, lipid raft microdomains regulate various functions mediated by GPCRs, such as vasopressin receptors and muscarinic receptors.

In salivary gland cells, muscarinic receptor-mediated water movement is largely mediated by three membrane events. The first is the activation of the muscarinic receptor GPCR. The second is SOCE after cytosolic Ca^{2+} pool depletion (Pani, Liu et al. 2013, Ambudkar 2016) and subsequent activation of Ca^{2+}-activated ion channels controlling the membrane potential (Romanenko, Nakamoto et al. 2007). The third is cytosolic Ca^{2+}-dependent translocation of AQP5 (Ishikawa, Cho et al. 2006). Lipid raft microdomains are considered to modulate these steps

significantly; however, the role of lipid raft microdomains in each step is not yet clearly understood, even though the role of lipid raft microdomains in vasopressin receptor-mediated AQP2 translocation in kidney has been relatively well studied.

This study sought to determine the lipid raft microdomains dependency of each activity-dependent AQP5 translocation step in salivary gland cells. MβCD disrupts lipid rafts by scavenging cholesterol (Koudinov and Koudinova 2001, Allen, Halverson-Tamboli et al. 2007). It investigated the effects of MβCD on muscarinic M3 receptor signaling and its downstream membrane events in mouse SMG cells.

Materials and Methods

Reagents

Carbachol, MβCD, and thapsigargin were purchased from Sigma (St. Louis, MO, USA), and fura-2-acetoxymethyl ester (fura-2/AM) was obtained from Molecular Probes (Eugene, OR, USA).

Primary SMG cell Preparation

Isolated mouse submandibular gland acinar cells were prepared as previously reported (Romanenko, Nakamoto et al. 2007). Briefly, mouse SMG tissue were surgically removed, finely minced with scissors, and digested for 5 min in 0.02% trypsin-EDTA (GIBCO) and 0.5 mg/mL collagenase (Sigma) in DMEM. The cells were triturated and centrifuged at 190× *g* for 1 min and then washed twice with serum-free DMEM. Acinar cells were attached to poly D-lysine-coated glass coverslips.

Cytosolic Free Ca^{2+} Measurement

The cytosolic free Ca^{2+} concentration ($[Ca^{2+}]_i$) was determined using the fluorescent Ca^{2+} indicator fura-2/AM, as previously described (Lee, Jo et al. 2017). Briefly, cells on coverslips were mounted onto the inverted microscope (Olympus IX70, Tokyo, Japan) and perfused continuously at 2 mL/min by a bath solution containing 140 mM NaCl, 5 mM KCl, 1 mM $MgCl_2$, 2 mM $CaCl_2$, 10 mM HEPES, and 10 mM glucose (pH 7.2). Fluorescence ratios were monitored with dual excitation at 340 nm and 380 nm and emission at 500 nm.

Cell Viability Assay

Cell viability was determined using the trypan blue exclusion assay. The cells were treated with 10 mM MβCD for 30 min, harvested, and added to 0.4% trypan blue (Sigma). The percentage of viable (trypan blue-unstained) cells was measured by counting the cells under the microscope.

Electrophysiological Recording

Whole-cell patch-clamp recordings were obtained using a HEKA EPC-9 amplifier (HEKA Elektronik, Lambrecht, Germany). The patch pipettes (3−6 MΩ resistance) were filled with 135 mM K-glutamate, 5 mM EGTA, 3 mM $CaCl_2$, and 10 mM HEPES, pH 7.2. The external solution contained 150 mM Na-glutamate, 5 mM K-glutamate, 2 mM $CaCl_2$, 2 mM $MgCl_2$, and 10 mM HEPES, pH 7.2. The stimulation protocol to generate current-voltage (I–V) relationships consisted of 40-ms voltage steps from −110 to +70 mV in 20-mV increments starting from a holding potential of −60 mV. Data were acquired and analyzed using PATCHMASTER software (HEKA Elektronik).

Analysis of AQP5 Protein Expression by Flow Cytometry

To evaluate the translocated AQP5 surface expression, we used flow cytometry in non-permeabilized cells performed as reported previously (Wang, Wee et al. 2016). Briefly, mice SMG single cells were obtained by mashing using a 100 μm cell strainer, followed by washing the cell strainer twice with 5 mL of 0.5% BSA in PBS. The cells were then centrifuged at 190 × *g* and washed twice with 0.5% BSA in PBS.

The cells were fixed with 4% formaldehyde, washed, and blocked 2% BSA in PBS. After blocking, the cells were washed and resuspended in 100 μL Alexa Fluor 647 conjugated AQP5 antibody (Abcam, ab215225, 1:500), and incubated for 30 min at 4 ℃ in the dark. All of the washing steps were carried out using 1% FBS in PBS as washing buffer, followed by centrifugation (8000 rpm, 1 min, 4 ℃). The labeled cells were kept on ice until analysis. The cell samples were then acquired on a FACSVerse flow cytometer equipped with FACSUITE software (BD Biosciences, San Jose, CA, USA).

Data Analysis

All quantitative data are expressed as mean ± SEM. Differences were determined by one-way analysis of variance (ANOVA) and considered significant when $p < 0.05$.

Results

Depletion of cholesterol by MβCD treatment did not affect cell viability in salivary cells.

Previous studies confirmed whether MβCD treatment depletes cholesterol in human salivary gland (HSG) cells, treatment with 10 mM MβCD for 30 min decreased the amount of cholesterol in HSG cells. It has revealed that 10 mM MβCD for 30 min is enough for cholesterol depletion in salivary cells.

Then whether this treatment has the cell toxicity was tested. Cell viability using trypan blue assay unchanged before and after MβCD treatment in both isolated mouse SMG cell (Figure 1A) and HSG cell line (Figure 1B). Moreover, morphology of HSG cell with MβCD treatment was unchanged (Figure 1C).

MβCD preincubation inhibited muscarinic intracellular Ca^{2+} increases without any effect on thapsigargin-mediated intracellular Ca^{2+} in SMG cells

Next, it investigated the effect of MβCD treatment on intracellular Ca^{2+} signaling in mouse SMG cells. A 30-min preincubation with 10 mM MβCD inhibited the intracellular Ca^{2+} increase triggered by carbachol ($t(52) = 2.20$, $p < 0.05$) (Figure 2B). However, MβCD incubation had no effect on the intracellular Ca^{2+} increase induced by thapsigargin, a sarcoplasmic reticular Ca^{2+}-ATPase (SERCA) inhibitor ($t(60) = 0.09$, $p = 0.93$) (Figure 2D). Considering that thapsigargin depletes the intracellular calcium pool and induces SOCE, these results indicate that preincubation with MβCD suppresses only GPCR activation without affecting SOCE activity.

MβCD preincubation increased the BK channel activity in salivary gland cells

When intracellular Ca^{2+} is increased by GPCR activation in the salivary gland, a series of Ca^{2+}-activated ion channels is activated. BK channels are present in the cholesterol-enriched lipid raft domain (Dopico, Bukiya et al. 2012). It estimated changes in BK channel activity by cholesterol depletion in isolated mouse SMG acinar cells using whole-cell patch clamp recording. Interestingly, preincubation of cells with 10 mM MβCD for 30 min increased K^+ current (Figure 3A), which were inhibited by the BK inhibitor paxilline (MβCD, $F(1,38) = 17.99$, $p < 0.001$; paxilline, $F(1,38) = 59.41$, $p < 0.001$; mV, $F(9,342) = 127.19$, $p < 0.001$) (Figure 3B). These results imply that salivary BK channel activity is increased by lipid raft disruption.

MβCD preincubation did not directly affect AQP5 translocation in SMG cells

Muscarinic Ca^{2+} signaling triggers the membrane trafficking of AQP5, a water channel protein in the salivary glands (Kim, Park et al. 2009, Lee, Gauna et al. 2013, Delporte 2014). To determine the effect of MβCD on aquaporins, it analyzed the membrane surface expression level of AQP5 by flow cytometry experiment. MβCD treatment marginally decreased the carbachol-induced AQP5 translocation (Figure 4C). Interestingly, MβCD treatment did not inhibit thapsigargin-induced AQP5 translocation (Figure 4D). These results suggest that the MβCD-mediated change in the salivary AQP5 translocation is mainly due to the decrease in muscarinic receptor-induced Ca^{2+} signaling.

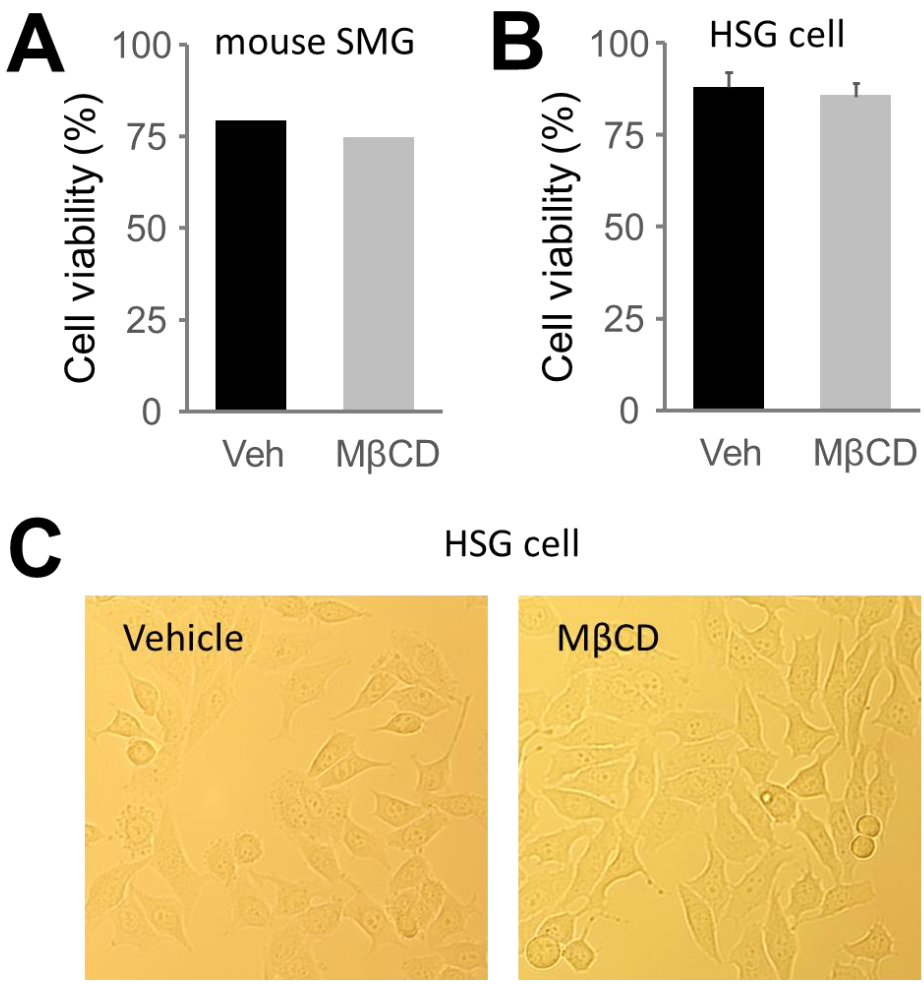
A
mouse SMG
Cell viability (%)
100
75
50
25
0
Veh
MβCD
B
HSG cell
Cell viability (%)
100
75
50
25
0
Veh
MβCD
C
HSG cell
Vehicle
MβCD

Figure 2-1. Depletion of cholesterol by MβCD treatment unchanged cell viability and morphology in salivary cells

A and B. Cells were incubated with 10 mM MβCD for 30 min then tested for cell viability using trypan blue assay in isolated mouse SMG cells (A) and HSG cells line (B).

C. The cell images of HSG cells before and after MβCD treatment.

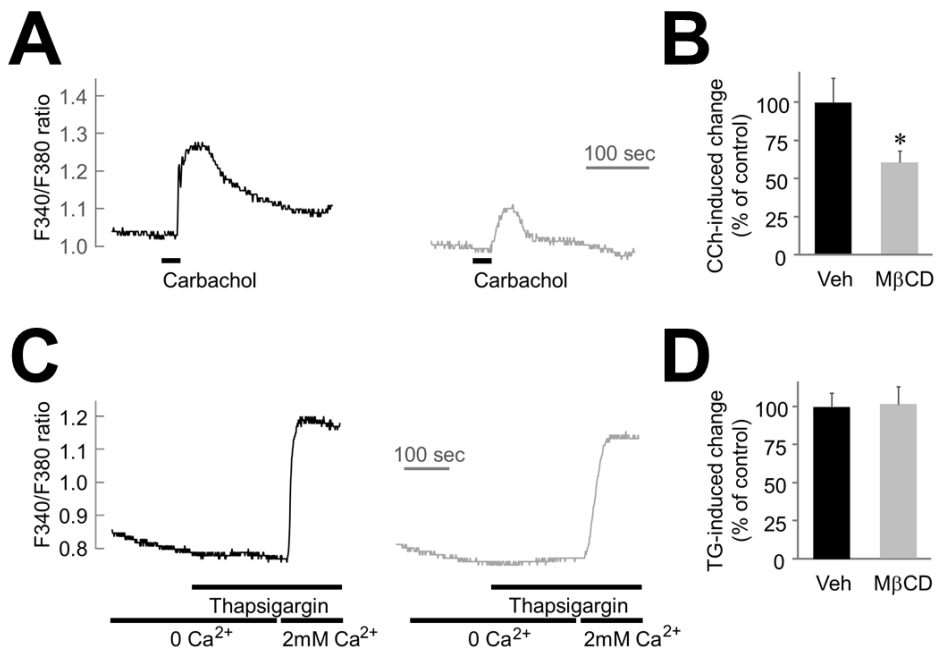
A
F340/F380 ratio
1.4
1.3
1.2
1.1
1.0
Carbachol
100 sec
Carbachol
B
CCh-induced change
(% of control)
100
75
50
25
0
*
Veh
MβCD
C
F340/F380 ratio
1.2
1.1
1.0
0.9
0.8
Thapsigargin
0 Ca2+
2mM Ca2+
100 sec
Thapsigargin
0 Ca2+
2mM Ca2+
D
TG-induced change
(% of control)
100
75
50
25
0
Veh
MβCD

Figure 2-2. Preincubation with MβCD inhibits carbachol-induced Ca^{2+} increase but not thapsigargin-induced Ca^{2+} increase

A. Representative Ca^{2+} imaging traces in SMG cells isolated from mice. Cells were treated with 100 μM carbachol with (black trace) or without (gray trace) 10 mM MβCD preincubation for 30 min.

B. Quantification of F340/F380 changes shows the percentage of all cells that responded to CCh with (black bar, n = 27 cells) or without (gray bar, n = 27 cells) 10 mM MβCD preincubation for 30 min. Data are presented as mean ± sem. *$p < 0.01$.

C. Representative Ca^{2+} imaging traces in mouse SMG cells. Vehicle (black trace) or MβCD (gray trace) preincubation cells were incubated in Ca^{2+}-free buffer and stimulated with 1 μM thapsigargin and then in 2.2 mM Ca^{2+}-containing buffer.

D. Quantification of F340/F380 changes shows the percentage of all cells that responded to thapsigargin with (black bar, n = 32 cells) or without (gray bar, n = 30 cells) 10 mM MβCD preincubation for 30 min.

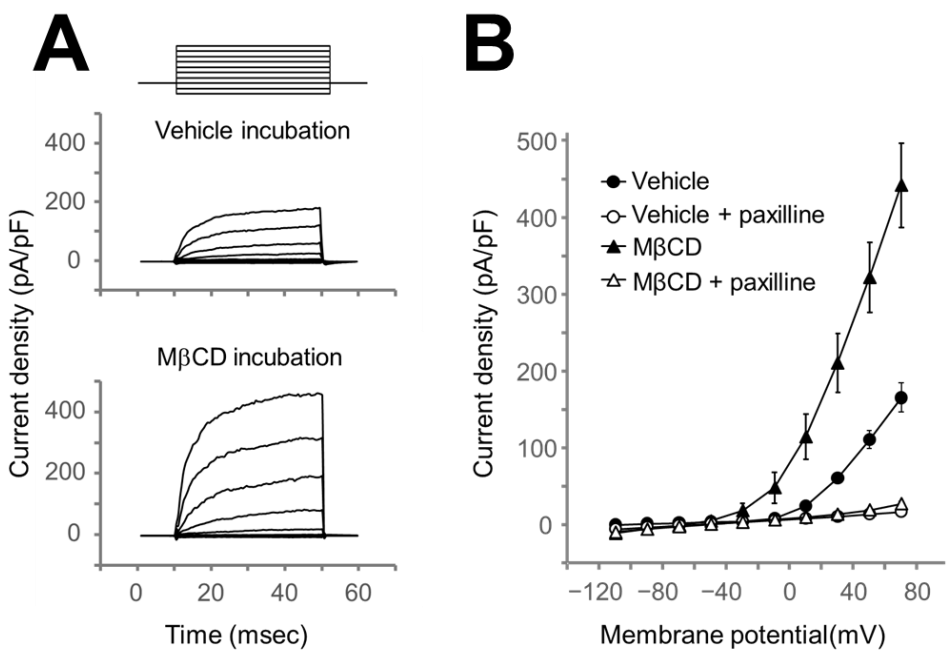
A
Vehicle incubation
MβCD incubation
Current density (pA/pF)
400
200
0
0
20
40
60
Time (msec)
B
Vehicle
Vehicle + paxilline
MβCD
MβCD + paxilline
Current density (pA/pF)
500
400
300
200
100
0
−120
−80
−40
0
40
80
Membrane potential(mV)

Figure 2-3. Preincubation with MβCD increases BK channel current in single SMG cells

A. Typical current traces were obtained in the control cells and those preincubated with 10 mM MβCD for 30 min. Currents were recorded immediately (15–20 s) after achieving whole-cell mode. The pulse protocol is shown as the graph insert.

B. Average I-V relations of current amplitudes measured at the end of 40 ms pulses to the indicated potentials in the absence (●) or presence (▲) of 10 mM MβCD. Open circle (○) and open triangle (△) plots were obtained after addition of 1 μM paxilline, a BK channel inhibitor. Each point represents the mean ± SEM (n = 10 or 11).

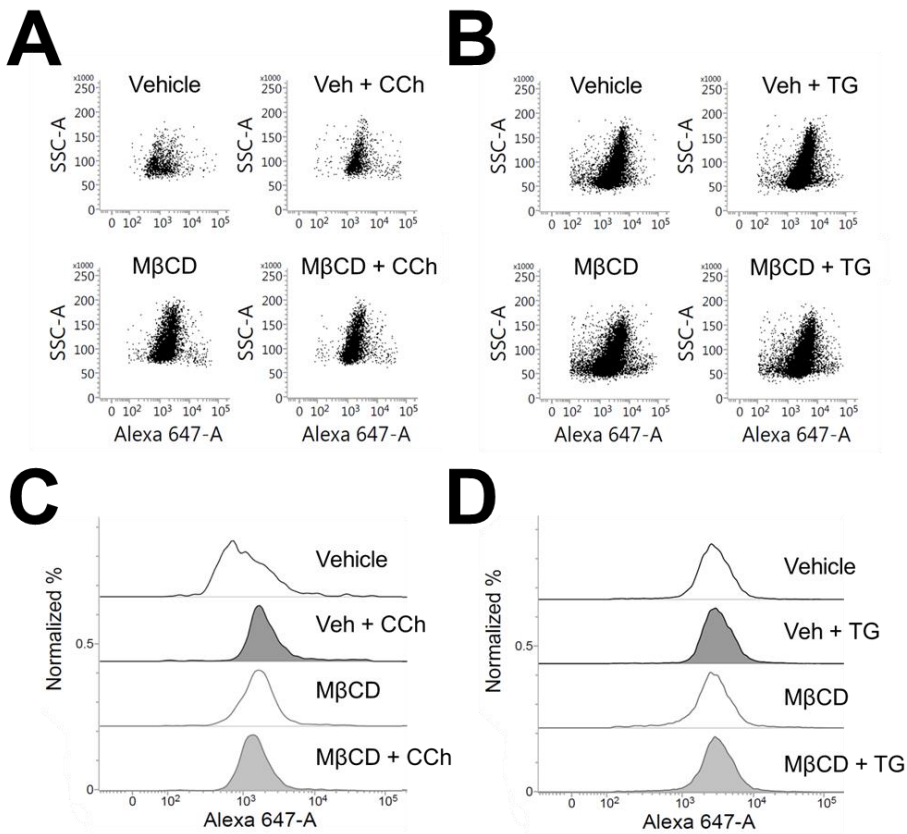
A
Vehicle
Veh + CCh
MβCD
MβCD + CCh
SSC-A
Alexa 647-A
B
Vehicle
Veh + TG
MβCD
MβCD + TG
SSC-A
Alexa 647-A
C
Normalized %
Vehicle
Veh + CCh
MβCD
MβCD + CCh
Alexa 647-A
D
Normalized %
Vehicle
Veh + TG
MβCD
MβCD + TG
Alexa 647-A

Figure 2-4. MβCD incubation does not directly affect AQP5 translocation

Representative dot plots (A and B) and histograms (C and D) from flow cytometry analysis represent the surface expression of AQP5 in the mouse isolated SMG cell. The cells were treated with or without 10 mM MβCD preincubation for 30 min and then challenged with 100 μM carbachol (A and C) or 1 μM thapsigargin (B and D).

Discussion

The physiological role of lipid rafts to optimize the functional cellular environment by maintaining membrane protein location and proximity between key functional players has received much scientific attention. In particular, the lipid raft mediates the physical association of GPCRs and downstream signal transduction factors. Thus, the lipid raft is more important in salivary cells that function based on polarity and those that function through several membrane events compared to their counterparts. However, the effects of the lipid raft on membrane events in salivary glands have not yet been clearly determined.

This study aimed to understand the role of lipid rafts in salivary function. Muscarinic M3 receptor-mediated Ca^{2+} signaling plays an important role in AQP5 translocation in salivary gland cells (Jin, Hwang et al. 2012, Lee, Gauna et al. 2013). The muscarinic mechanism in the plasma membrane includes M3 receptor activation, SOCE activation, and AQP5 translocation. In addition, muscarinic M1 and M3 receptors and (voltage-gated) K^+ channels exist in the membrane lipid raft and functionally couple in neurons (Sebastiao, Colino-Oliveira et al. 2013) and HEK cells (Oldfield, Hancock et al. 2009). In addition, a BK channel also exists in the lipid raft (Weaver, Olsen et al. 2007, Riddle, Hughes et al. 2011, Tajima, Itokazu et al. 2011). It is expected that the muscarinic receptors and BK channels of salivary gland cells also exist in the lipid raft. These results show that MβCD-mediated lipid raft depletion inhibited carbachol-induced intracellular Ca^{2+} increase. The effect of lipid raft microdomains on GPCR activation has been reported in many cells with frequent signal transduction (e.g., neurons). These findings suggest that lipid raft microdomains optimize GPCR signaling in salivary gland cells.

Interestingly, the result revealed that the thapsigargin-triggered Ca^{2+} increase was not affected by MβCD. Thapsigargin is a SERCA inhibitor that induces Ca^{2+} pool depletion by inhibiting recharge of the cytosolic Ca^{2+} pool and subsequently induces SOCE without GPCR activation. Thus, these findings of different inhibitory effects on carbachol and thapsigargin imply that the lipid raft inhibits GPCR activation without affecting SOCE activity. However, there have been several previous reports that SOCE is affected by lipid rafts (Jardin, Salido et al. 2008, Galan, Woodard et al. 2010, Dionisio, Galan et al. 2011). It is suspected this discrepancy is due to the difference in SOCE characteristics. Despite the commonality of the triggering mechanism (i.e., intracellular Ca^{2+} pool depletion), SOCE characteristics depend on cell type. SOCE is mediated by a series of factors, including TRPC1, Orai1, and STIM1 (Ambudkar, de Souza et al. 2017). A previous study observed that thapsigargin-induced SOCE in PC12 cells is different from those in HL-60 cells and Jurkat T cells (Lee, Kim et al. 2017). Therefore, we concluded that lipid rafts do not affect SOCE in salivary gland cells.

It found that disruption of lipid rafts increased BK channel activity. It has previously been shown that cholesterol modulates BK channel activity by controlling lipid rafts (Yang, Zhang et al. 2015). The cholesterol depletion-mediated increase in BK channel current activity has been found in IGR39 human melanoma cells (Tajima, Itokazu et al. 2011) and rat vascular smooth muscle cells (Bukiya, Vaithianathan et al. 2011, Riddle, Hughes et al. 2011). It has been reported that cholesterol treatment reduces the open probability of the BK channel in rat cerebral artery myocytes (Bukiya, Belani et al. 2011). However, it also has been reported that the BK channel current was decreased by MβCD in D54-MG and

U251 glioma cell lines (Weaver, Olsen et al. 2007), implying that the relationship between lipid raft microdomains and BK channel activity depends on cell type. Disruption of the cholesterol-enriched lipid raft structure is expected to modulate the activity by controlling the gating of the BK channel (Dopico, Bukiya et al. 2012), but a clearer understanding of the molecular mechanism remains to be elucidated.

Finally, it examined the effect of lipid raft depletion on AQP5 translocation to the plasma membrane. Interestingly, MβCD did not affect carbachol- and thapsigargin-induced AQP5 translocation. Given that MβCD did not cause a thapsigargin-induced Ca^{2+} increase or an increase in AQP5 translocation, these results indicate that the lipid raft microdomain does not affect the translocation of AQP5. It has been reported that lipid raft microdomains are involved in targeting aquaporins (Asakura, Ueda et al. 2014), and the colocalization of the lipid raft markers flotillin and AQP5 is increased during treatment with muscarinic receptor agonists and Ca^{2+} ionophores (Ishikawa, Cho et al. 2006). However, it is unclear how lipid raft microdomains affect these sequential events in membranes (i.e., from muscarinic receptor activation to AQP5 translocation). These results clearly show that MβCD inhibits carbachol-induced AQP5 translocation, mainly at the receptor level.

Lipid-lowering medications prescribed for hypercholesterolemia to lower blood cholesterol include HMG-CoA reductase inhibitors, commonly referred to as statins (Sirtori 2014). Interestingly, it has been reported that xerostomia, along with lichenoid and aphthae, is frequently found in patients receiving a statin prescription (Habbab, Moles et al. 2010). In addition, when statin treatment was stopped in dry mouth patients undergoing statin treatment, dry mouth symptoms were found to be

relieved. Our results, elucidating the relationship between cholesterol-depletion and salivary signaling, strongly suggest the causative mechanism of dry mouth in lipid-lowering medications.

Taken together, we examined the effects of lipid rafts on muscarinic signaling and found that lipid raft microdomains regulate GPCR and BK channels in the salivary gland cells. This study will help others understand the molecular target of lipid raft microdomain on the muscarinic signaling-mediated water secretion and will contribute to a better understanding of the cellular and molecular mechanisms of lipid raft microdomains in modulating exocrine functions.

Chapter 3.

The regulation of neuro-exocrine common factors on Ca^{2+} signal and Ca^{2+}-activated ion channels in mouse SMG cells

Introduction

The secretion function of exocrine glands is controlled finely by extracellular signals such as nerves (Proctor and Carpenter 2007). Salivary exocrine glands are supplied by parasympathetic nerves which release acetylcholine that binds to muscarinic receptors. Interaction of neuron and exocrine cells is similar to signaling in neurons, in that it composed signaling molecules secretion and its receptor. Neurotransmitter release and receptor signal in neurons were regulated through a variety of mechanisms by various factors. If a functional regulator in the neuron is expressed in another cell, it is possible to control cell-to-cell communication in the cell. For example, muscarinic receptors expressed in many brain regions such as cerebral cortex and hippocampus regulate neuron-to-neuron communication by acetylcholine secreted from cholinergic neuron. Similarly, muscarinic receptors expressed also in peripheral organs such as salivary gland mediate neuron-to-organ communication evoking parasympathetic responses. Therefore, the factors expressed commonly in neuron and salivary glands are likely to regulate the physiological function of salivary gland.

Recent transcriptomic studies have revealed that some of the genes controlling the neuronal functions are also expressed in the salivary glands (Gluck, Min et al. 2016, Gao, Oei et al. 2018, Song, Min et al. 2018, Oyelakin, Song et al. 2019, Saitou, Gaylord et al. 2020, Sekiguchi, Martin et al. 2020). These studies contributed to identifying the type of salivary glands (Gao et al., 2018; Saito et al., 2020), the diversity of cells composed salivary gland (Oyelakin et al., 2019) and the developmental mechanism of salivary gland (Gluck et al., 2016; Sekiguchi et al., 2020; Saitou et al., 2020). Surprisingly, it demonstrated a variety of genes

expressed in submandibular gland are also detected in neuron (Gluck, Min et al. 2016, Sekiguchi, Martin et al. 2020). However, whether the neuron-salivary common factors regulate the function of salivary gland remains uncertain. This study may lead to novel approaches for identifying mechanisms in salivary gland disease.

Neuronal growth regulator 1 (NEGR1) has been associated with major depression (Maccarrone, Ditzen et al. 2013, Tamasi, Petschner et al. 2014, Dall'Aglio, Lewis et al. 2021), expressed high levels in brain regions such as cerebral cortex, diencephalon, hippocampus, and cerebellum (Miyata, Matsumoto et al. 2003). NEGR1 as a cell-adhesion molecule is an important role in the structural formation and development of synapse to promote synaptogenesis and dendrite formation. Additionally, it has been shown that NEGR1 is important for regulating receptor signaling in postsynaptic neurons and maintaining synaptic plasticity (Noh, Lee et al. 2019, Noh, Park et al. 2020). While expression or function of NEGR1 in salivary gland remains to be elucidated.

This study tried to elucidate salivary secretion in an animal model in which *Negr1* expression was suppressed and to identify changes in secretion mechanism through a physiological approach. It confirmed *Negr1* gene expressed in salivary gland is critical to maintain muscarinic Ca^{2+} signal and induce AQP5 translocation.

Materials and Methods

RNA isolation and RT-PCR

Total RNA was prepared from cerebral cortex, hippocampus, stomach, and SMG of C57BL/6 mouse and SMG of *Negr1* knock-out mouse. The tissues were homogenized in Trizol reagent (Ambion, USA) and RNA was extracted according to the manufacturer's protocol.

Complementary DNA was reverse-transcribed (RT) from 2 μg of total RNA primed with 10 pmole oligo-dT in 20 μl reaction containing SuperScript™ III Reverse Transcriptase (Thermo, 18080093). PCR was performed using Solg ™ 2X Taq PCR Smart mix 2 (SolGent, STD02-M50h), 1 μl of cDNA template from RT reaction, forward and reverse primers each at 0.8 μM in 20 μl reaction. The protocol consisted of incubation at 95ºC for 2 min followed by 35 cycles of 95ºC for 20 sec, 55ºC for 40 sec, 72ºC for 20 sec and extended at 72ºC for 5 min in SimpliAmp thermocycler (Applied biosystems, Life technologies, USA). All of the amplified reaction was electrophoresed on a 1.5% agarose gel. Mouse Negr1-specific PCR primers were designed as follows: 5'-gcttctgagcctgtgctctt-3' (forward) and 5'-cacttgtcacctccagcaaa-3' (reverse).

H&E staining

Hematoxylin-eosin staining was performed as described previously (Park et al., 2021). SMG samples were fixed in 4% paraformaldehyde overnight at 4°C and embedded in paraffin. Tissue sections (5 μm) were deparaffinized in xylene (DUKSAN Chemicals, UN1307) and rehydrated with ethanol (DUKSAN Chemicals, UN1170). The samples were stained with hematoxylin (Vector Labs, H-

3401) for 4 min and eosin (T&I, BEY-9005) for 2 min. Images from the sections were captured by a digital upright fluorescence microscope (DP72, Olympus BX51, Japan).

Mouse SMG cell preparation

Isolated mouse SMG cells were prepared as previously reported (Lee et al., 2021). Briefly, mouse submandibular glands were surgically removed, finely minced with scissors, and digested for 5 min in 0.02% trypsin-EDTA (GIBCO) and 0.5 mg/mL collagenase (Sigma) in serum-free DMEM. The cells were dispersed by trituration through a heat-polished pasteur pipette 10 times every 10 min using decreasing pore sizes (L-M-S). The cells were centrifuged at 190× *g* for 1 min and then washed twice with serum-free DMEM. The resuspended cells in serum-free media are filtered through 40 μm cell strainer (BD falcon, USA). The cells were attached to poly D-lysine-coated glass coverslips or 35 mm dish.

Ca^{2+} imaging

Ca^{2+} imaging was performed as previously described (Lee, Jo et al. 2017). Cells were isolated as described above and loaded with 2 μM fura-2/AM and 0.01% pluronic F-127 (Molecular Probes) for 40 min at 37℃. The cells on coverslips were mounted onto the inverted microscope (Olympus IX70) and perfused continuously at 2 mL/min by bath solution containing (mM) 140 NaCl, 5 KCl, 1 $MgCl_2$, 2 $CaCl_2$, 10 HEPES, and 10 glucose (pH 7.20). For recordings in Ca^{2+}-free conditions, Ca^{2+} was replaced with equivalent concentration of EGTA. All measurements were made at room temperature. Cells were illuminated with a 175-

W xenon arc lamp, and excitation wavelengths (340/380 nm) were selected by a Lambda DG-4 monochromator filter changer (Shutter Instrument). Intracellular free calcium concentration was measured by digital video microfluorometry with an intensified charge-coupled device (CCD) camera (CasCade; Roper Scientific) coupled to a microscope and software (Metafluor 6; Molecular Devices).

Electrophysiology

ANO1, BK, SOCE activities were measured in mouse salivary gland acinar cells using whole-cell patch-clamp techniques. For measuring ANO1 channel current (Jung et al. 2013), the patch pipette solution was contained within a solution containing (mM) 148 N-methyl-D-glucamine-Cl (NMDG-Cl), 10 EGTA, 7.4 $CaCl_2$, 3 MgATP, and 10 HEPES (pH 7.2). The external bath solution contained (mM) 146 NMDG-Cl, 1 $CaCl_2$, 1 $MgCl_2$, 10 HEPES, and 5 glucose (pH 7.4). The stimulation protocol to generate current–voltage relationships consisted of 500-ms voltage steps from −100 to +100 mV in 20-mV increments, starting from a holding potential of −60 mV. For measuring BK channel current (Lee et al. 2021), the patch pipette solution was contained within a solution containing (mM) 135 K-glutamate, 5 EGTA, 3 $CaCl_2$, and 10 HEPES (pH 7.2). The external bath solution contained (mM) 150 Na-glutamate, 5 K-glutamate, 2 $CaCl_2$, 2 $MgCl_2$, and 10 HEPES (pH 7.2). The stimulation protocol to generate current-voltage relationships consisted of 40-ms voltage steps from −110 to +70 mV in 20-mV increments starting from a holding potential of −70 mV. For measuring SOCE current (Sukumaran et al. 2019), the patch pipette solution was contained within a solution containing (mM) 150 Cesium methane sulfonate, 8 NaCl, and 10 HEPES (pH 7.2). The external bath

solution contained (mM) 145 NaCl, 5 CsCl, 1 $CaCl_2$, 1 $MgCl_2$, 10 HEPES, and 10 glucose (pH 7.3). With holding potential 0 mV, voltage ramps ranging from -100 mV to +100 mV and 100 milliseconds duration were delivered at 2 seconds intervals after whole-cell configuration was formed. Whole-cell patch-clamp recordings were obtained using a HEKA EPC-9 amplifier (HEKA Elektronik, Lambrecht, Germany). Data were acquired and analyzed using the PATCHMASTER software program (HEKA Elektronik).

Quantitative real-time PCR

To measure quantitative *Aqp5* mRNA in submandibular glands, we used previously described methods (Lee et al. 2019) and performed using the SYBR Premix Ex Taq (RR420A; Takara, Tokyo, Japan) and the QuantStudio™ real-time PCR detection system (Applied Biosystems, Waltham, MA, USA). cDNAs were amplified in 20 μl PCR reactions using 1 μl of RT reaction. Reactions with appropriate melting curve were selected for analysis and all primer sets were analyzed in triplicate. The *Gapdh* mRNA level was used as an internal control to normalize the values for transcript abundance of *Aqp5* genes. We performed four qRT-PCR experiments and averaged from triplicate analysis of each experiment.

AQP5 Surface Protein Expression by Flow Cytometry

To evaluate the surface AQP5 expression, we used flow cytometry performed as reported previously (Lee, Kim et al. 2021). Briefly, mice SMG single cells were obtained by grinding using a 100 μm cell strainer, followed by washing the cell strainer twice with 5 mL of 0.5% bovine serum albumin (BSA) in PBS. The cells

were then centrifuged at 190× g and washed twice with 0.5% BSA in phosphate-buffered saline (PBS). The cells were fixed with 4% formaldehyde after short treatment of CCh, washed, and blocked 2% BSA in PBS. After blocking, the cells were washed and resuspended in 100 μL Alexa Fluor 647 conjugated AQP5 antibody (Abcam, ab215225, 1:500), and incubated for 20 min at 4 ℃ in the dark. All of the washing steps were carried out using 1% FBS in PBS as washing buffer, followed by centrifugation (8000 rpm, 1 min, 4 ℃). The labeled cells were kept on ice until analysis. The cell samples were then acquired on a FACSVerse flow cytometer equipped with FACSUITE software (BD Biosciences, San Jose, CA, USA).

Results

Negr1 expression in SMG and normal morphology in *Negr1* KO mice

It examined whether *Negr1* was detected in mouse SMG by RT-PCR. The result indicated that *Negr1* expressed not only SMG but also brain (cerebral cortex and hippocampus) and stomach in mouse (Figure 1A). It estimated the structure and function of SMG using KO mice deleted *Negr1* gene to identify the role of NEGR1 in salivary gland. Compared to WT mice, the unchanged morphology of SMG tissue in *Negr1* KO mice is confirmed by H&E staining (Figure 1B). However, salivation of *Negr1* KO mice is dramatically reduced (data not shown). This result suggested that NEGR1 affects the function of salivation without change of structure or development.

Reduction of muscarinic Ca^{2+} signaling and SOCE in *Negr1* KO mice

To predict the molecular mechanism of salivation deficiency in *Negr1* KO mice, it estimated the muscarinic Ca^{2+} signaling which is a critical role in salivation. The peak of CCh-induced intracellular Ca^{2+} increase normalized the peak of ionomycin is declined in *Negr1* KO mice (Figure 2). Activation of muscarinic receptor mediates SOCE in salivary gland cells (Kann, Taubenberger et al. 2012). Tg as a SERCA inhibitor induced SOCE, the peak of intracellular Ca^{2+} increase by Tg is decreased also in *Negr1* KO mice (Figure 3). It suggested that SOCE reduction in *Negr1* KO mice, SOCE currents using whole-cell recording confirmed SOCE diminished significantly in *Negr1* KO mice (Figure 4). These results showed NEGR1 regulated muscarinic Ca^{2+} signaling and SOCE in salivary gland cells.

Changes of calcium-activated ion channels activity in *Negr1* KO mice

It observed the NEGR1 effect on the activity of calcium-activated ion channels which are subordinate molecules of intracellular Ca^{2+} signaling. ANO1 channels as calcium-activated Cl^- channels expressed in acinar cells induce efflux of chloride ions, it is a driving force of primary fluid secretion (Romanenko, Catalan et al. 2010). And BK channels as calcium-activated K^+ channels hyperpolarized the cell membrane in acinar cell, it induced chloride ion flow (Romanenko, Thompson et al. 2010). ANO1 channel currents in WT and *Negr1* KO mice, the activity of ANO1 channel is similar in both (Figure 5A). While the activity of BK channel is increased markedly in *Negr1* KO mice (Figure 5B). The BK channel expression level of mRNA (*Kcnma1*) and membrane surface protein were unchanged in both mice (Figure 6). However, the mRNA expression level of auxiliary beta 2 subunit (*Kcnmb2*) was increased notably in *Negr1* KO mice (Figure 6B), it predicted increased current of BK channel (Lippiat, Standen et al. 2003).

Decreased surface AQP5 expression in *Negr1* KO mice

Finally, it estimated the expression difference of AQP5, associated with water movement by a transcellular pathway in salivary acinar cell. Total mRNA expression of *Aqp5* by quantitative PCR was not changed in *Negr1* KO mice (Figure 7A, B). However, the cell surface expression of AQP5 by flow cytometry is decreased in *Negr1* KO mice (Figure 7C, D). These results indicated that reduction of AQP5 membrane translocation, it decreased salivation in *Negr1* KO mice.

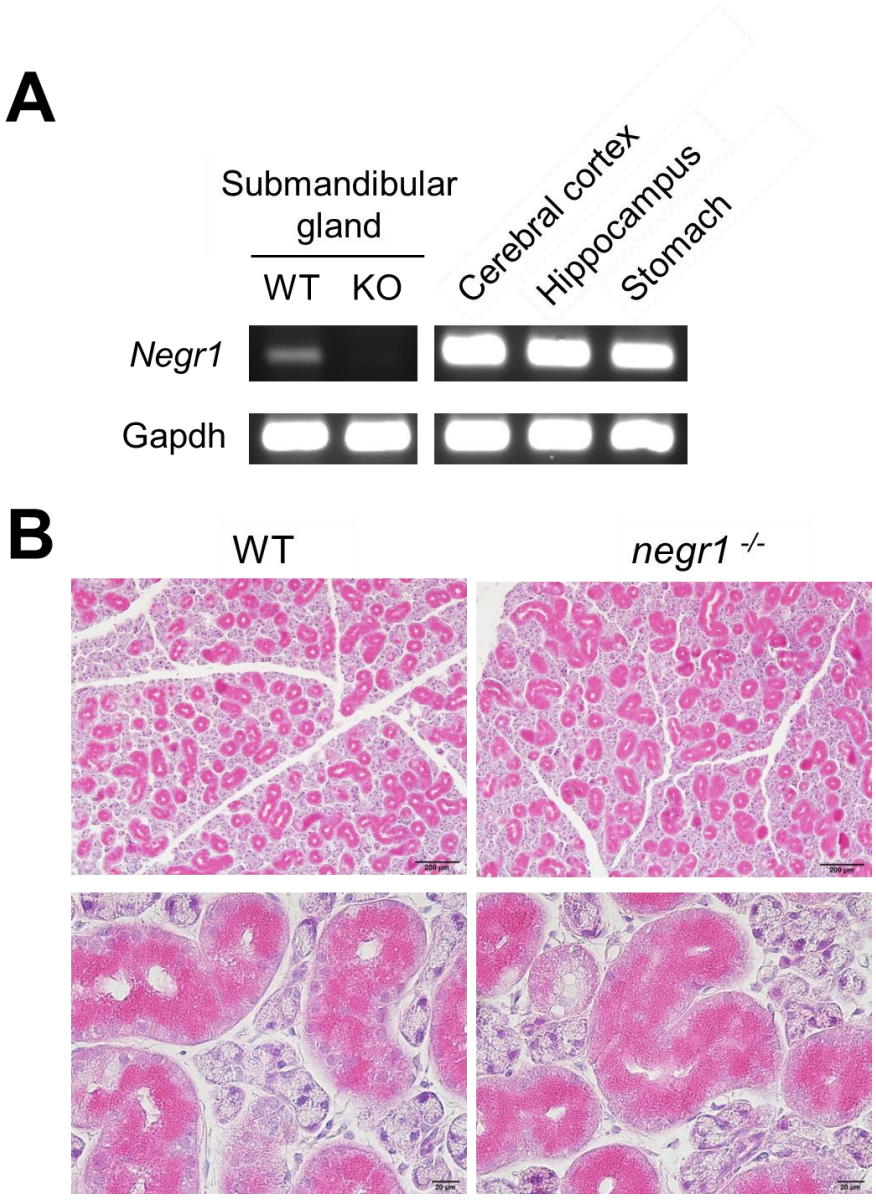
A
Submandibular gland
WT
KO
Cerebral cortex
Hippocampus
Stomach
Negr1
Gapdh
B
WT
negr1 -/-

Figure 3-1. Normal morphology gland but decreased salivation in *Negr1* knock-out mice

A. Messenger RNA expression levels of *Negr1* genes were monitored in the mouse submandibular glands, cerebral cortex, hippocampus, and stomach of WT and *Negr1* KO mice. *Gapdh*; Glyceraldehyde 3-phosphate dehydrogenase, a housekeeping gene as a PCR positive control.

B. The images of mouse SMG gland tissue by H&E staining. The gross morphology of the SMG did not change appreciably between the WT and *Negr1* KO mice.

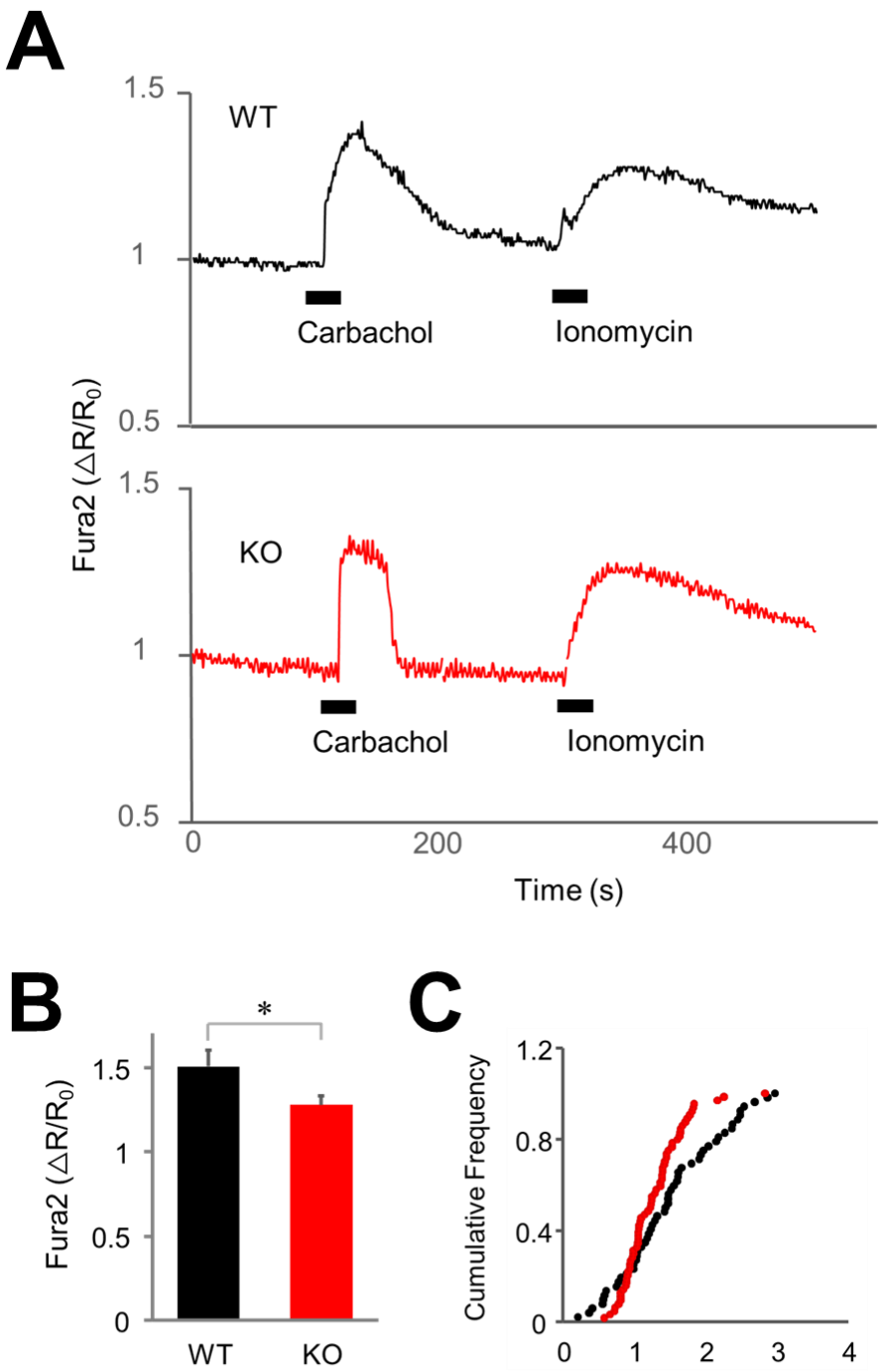
A
1.5
WT
1
Carbachol
Ionomycin
0.5
Fura2 (ΔR/R0)
1.5
KO
1
Carbachol
Ionomycin
0.5
0
200
400
Time (s)
B
*
Fura2 (ΔR/R0)
1.5
1
0.5
0
WT
KO
C
Cumulative Frequency
1.2
0.8
0.4
0
0
1
2
3
4

Figure 3-2. Change of intracellular Ca^{2+} increase induced by carbachol in *Negr1* KO mice SMG cells

Fura-2/AM loaded cells treated with 100μM CCh for 30 sec and washed then treated with 3uM ionomycin for 30 sec.

A. Typical Ca^{2+} imaging traces showing the Fura-2 fluorescence ratio of SMG cells in WT and *Negr1* KO mice.
B. Bar graph indicated normalized CCh-induced Ca^{2+} increase peak by the peak of ionomycin.
C. Cumulative frequency plot showed all reactions from WT (n = 52) and *Negr1* KO (n = 64) mice.

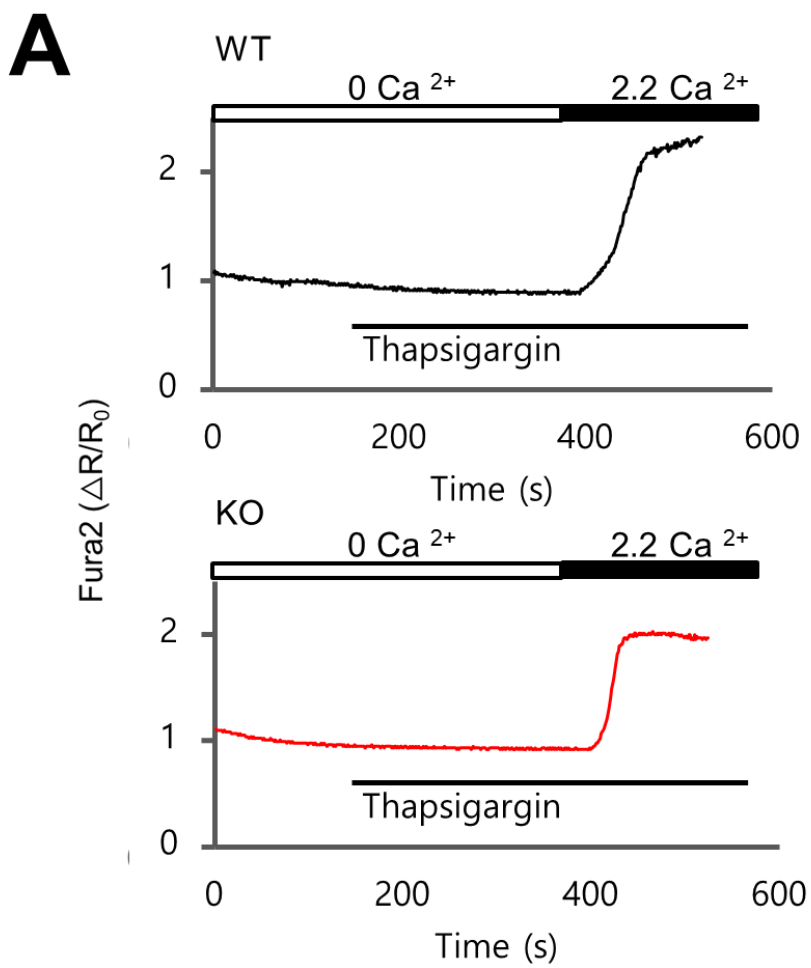
A
WT
0 Ca 2+
2.2 Ca 2+
2
1
0
Thapsigargin
0
200
400
600
Time (s)
Fura2 (△R/R0)
KO
0 Ca 2+
2.2 Ca 2+
2
1
0
Thapsigargin
0
200
400
600
Time (s)

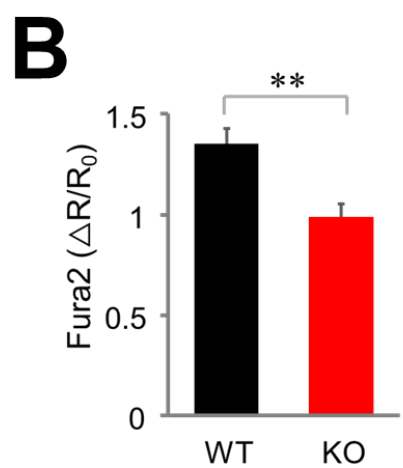
B
**
1.5
1
0.5
0
Fura2 (△R/R0)
WT
KO

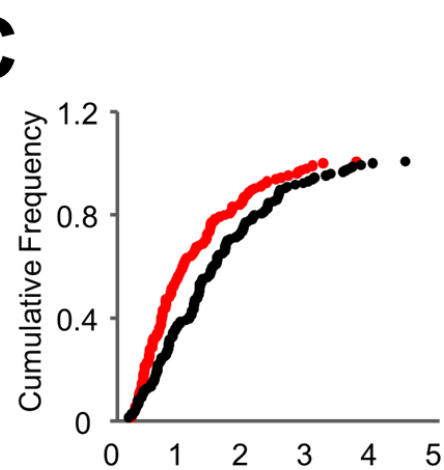
C
1.2
0.8
0.4
0
Cumulative Frequency
0
1
2
3
4
5

Figure 3-3. Change of intracellular Ca^{2+} increase induced by thapsigargin in *Negr1* KO mice SMG cells

Fura-2/AM loaded cells were incubated in Ca^{2+} free HBSS solution and stimulated with 1μM Tg and then in 2.2 mM Ca^{2+} containing HBSS solution to induce SOCE.

A. Typical Ca^{2+} imaging traces showing the Fura-2 fluorescence ratio of SMG cells in WT and *Negr1* KO mice.
B. Bar graph indicated the peak of Ca^{2+} increase by Tg in Ca^{2+} containing HBSS solution.
C. Cumulative frequency plot showed all reactions from WT (n = 143) and *Negr1* KO (n = 144) mice.

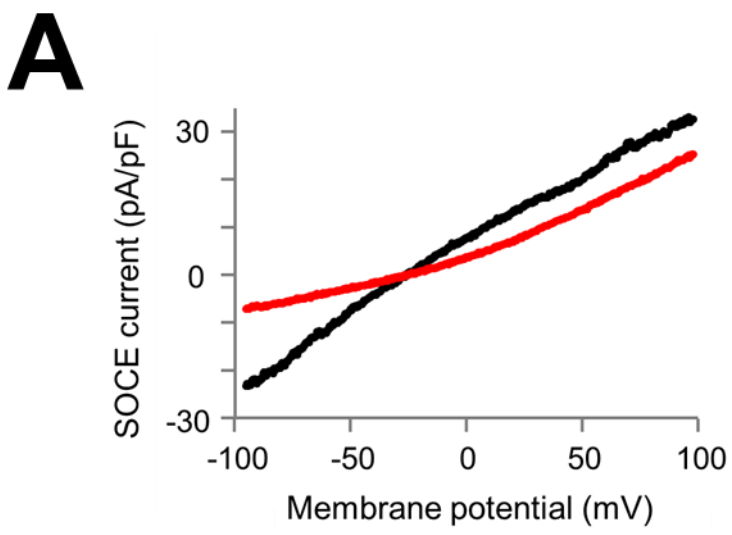
A
SOCE current (pA/pF)
30
0
-30
-100
-50
0
50
100
Membrane potential (mV)

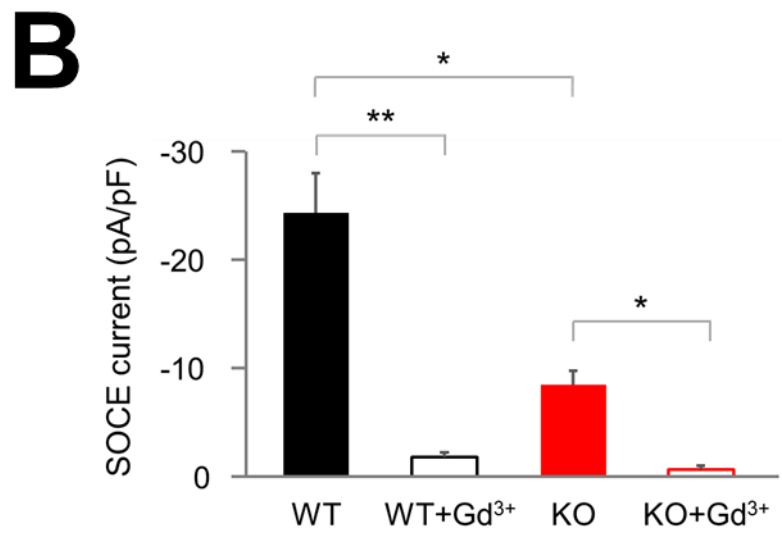
B
SOCE current (pA/pF)
-30
-20
-10
0
*
**
*
WT
WT+Gd3+
KO
KO+Gd3+

Figure 3-4. SOCE currents were decreased in *Negr1* KO mice.

The amplitude of SOCE currents recorded in whole-cell experiments measured at each ramp after the application of 1 uM of Tg.

A. I–V curves of currents induced by the depletion of Ca^{2+} store with 1 uM of Tg in WT and *Negr1* KO submandibular gland cells. The currents evoked by the −100 mV to 100 mV.

B. The quantitation of current intensity at −100 mV are shown as bar graphs. Gadolinium (Gd^{3+}) as a SOCE inhibitor blocks all SOCE currents.

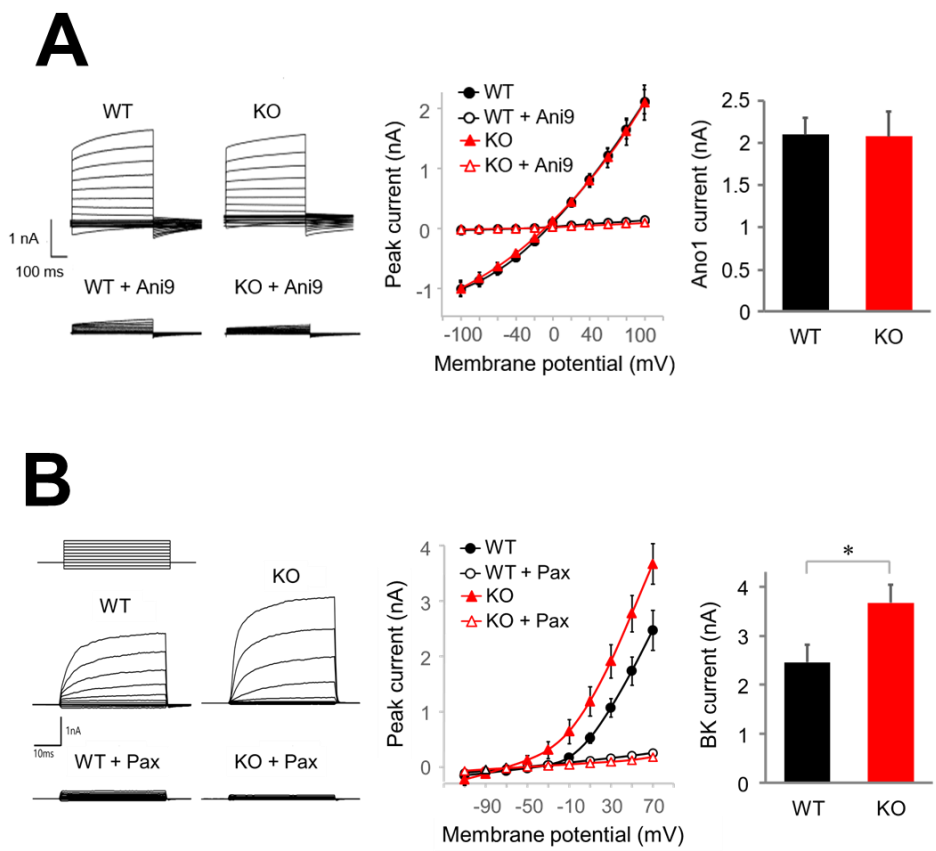
A
WT
KO
1 nA
100 ms
WT + Ani9
KO + Ani9
WT
WT + Ani9
KO
KO + Ani9
Peak current (nA)
Membrane potential (mV)
Ano1 current (nA)
WT
KO
B
WT
KO
1nA
10ms
WT + Pax
KO + Pax
WT
WT + Pax
KO
KO + Pax
Peak current (nA)
Membrane potential (mV)
BK current (nA)
*
WT
KO

Figure 3-5. Whole-cell currents of calcium-activated ion channels were measured in SMG acinar cells of WT and *Negr1* KO mice.

A. Representative current traces of ANO1 channel. The cell was held at -60 mV, and the depolarizing pulses from -100 to +100 mV were delivered in 20-mV increments. The I-V relationship and bar graph of the peak current of ANO1 channel at +100 mV showed no change. Ani9; a specific Ano1 inhibitor.

B. Typical current traces of BK channel. The I-V curves were obtained by step pulses (voltage interval; 20mM, duration; 40ms) from -110 mV to +70 mV. Bar graph showing peak current of BK channel at +70 mV. Pax; paxilline as a specific BK channel inhibitor.

Mean ± SEM. *Significantly different from the control.

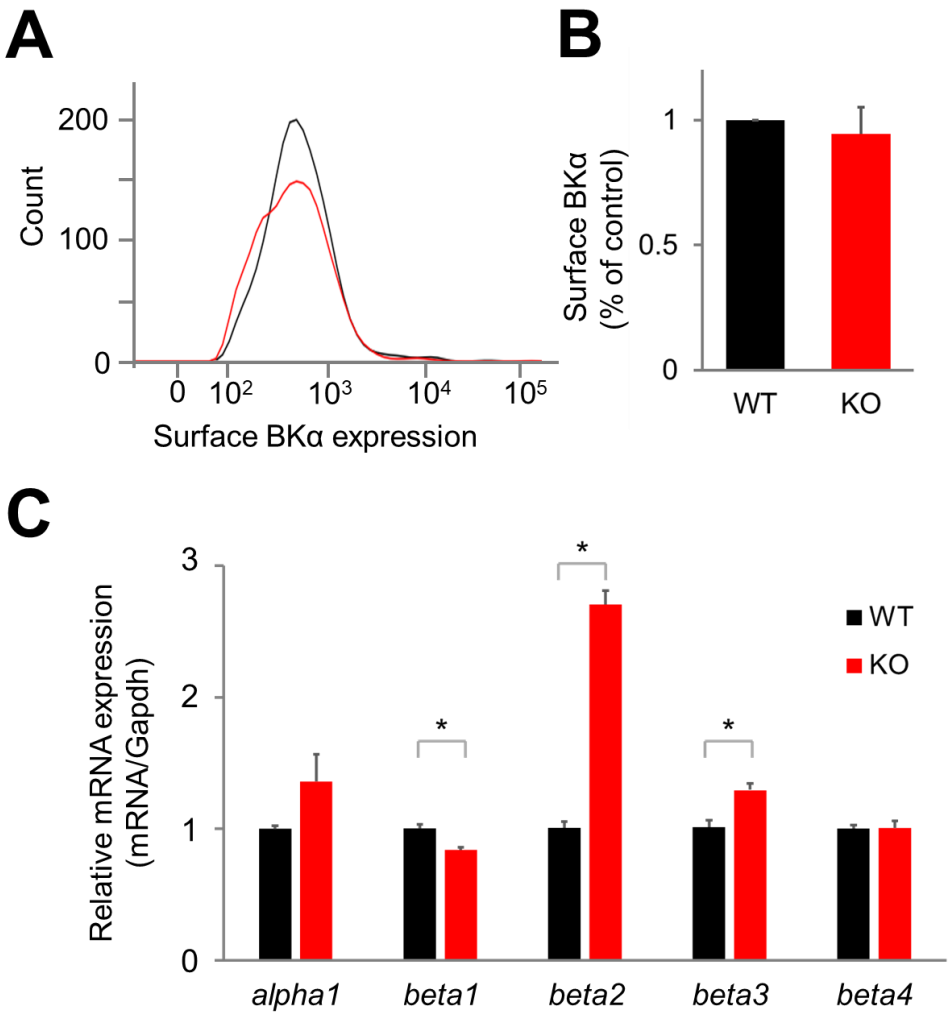
A
Count
200
100
0
0
10^2
10^3
10^4
10^5
Surface BKα expression
B
Surface BKα
(% of control)
1
0.5
0
WT
KO
C
Relative mRNA expression
(mRNA/Gapdh)
3
2
1
0
*
*
*
WT
KO
alpha1
beta1
beta2
beta3
beta4

Figure 3-6. Increased BK currents induced auxiliary beta subunit of BK channel.

A. Representative histogram BK surface expression of SMG cells in WT and *Negr1* KO mice measured by flow cytometry.

B. Bar graph showing the relative expression of surface BK expression from flow cytometry analysis in WT and *Negr1* KO mice.

C. Relative mRNA expression levels of BK channel subunits in SMG tissue from WT and *Negr1* KO mice. alpha1; main alpha subunit of BK channel, beta; auxiliary beta subunits of BK channel.

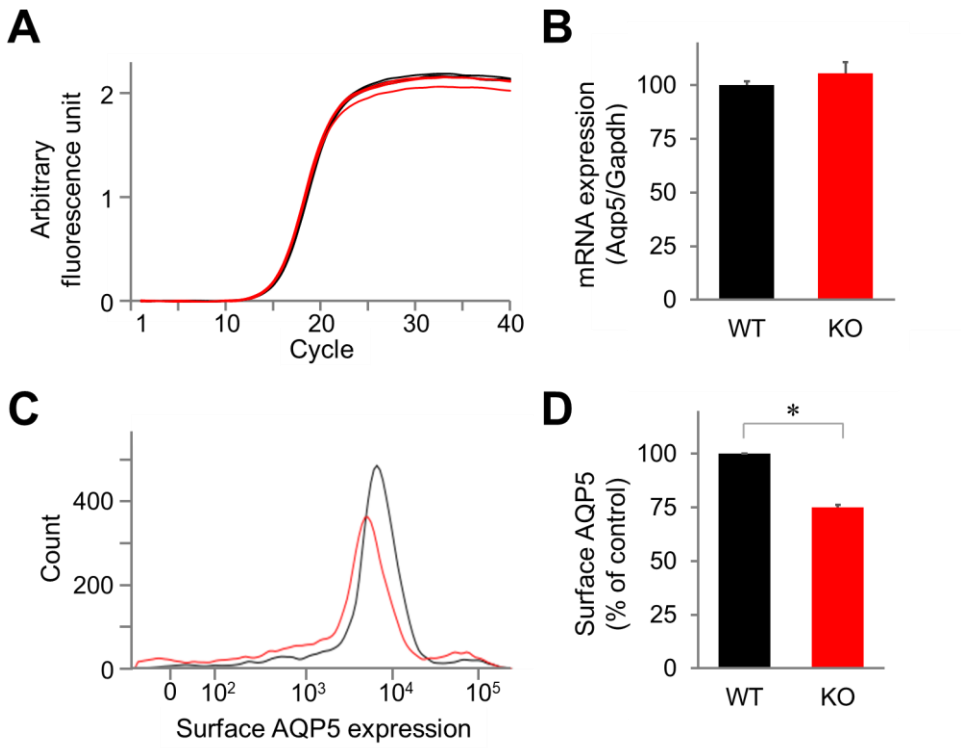
A
Arbitrary fluorescence unit
2
1
0
1
10
20
30
40
Cycle
B
mRNA expression (Aqp5/Gapdh)
100
75
50
25
0
WT
KO
C
Count
400
200
0
0
10^2
10^3
10^4
10^5
Surface AQP5 expression
D
Surface AQP5 (% of control)
*
100
75
50
25
0
WT
KO

Figure 3-7. Expression levels of AQP5 in whole SMG tissue of WT and *Negr1* KO mice

Quantitative RT-PCR analysis of *Aqp5* mRNA and flow cytometry analysis of AQP5 surface expression in SMG cells from WT and *Negr1* KO mice.

A. Real-time change in fluorescence with PCR cycle number in a representative of qRT-PCR experiment. The result was determined in technical triplicates and data are plotted as lines.
B. Relative expression of *Aqp5* mRNA in SMG cells from WT and *Negr1* KO mice was normalized to *Gapdh* reference gene.
C. Representative histogram AQP5 surface expression of SMG cells in WT and *Negr1* KO mice measured by flow cytometry.
D. Quantification of AQP5 surface expression of submandibular gland cells in WT and *Negr1* KO mice by flow cytometry. * $p < 0.05$.

Discussion

It demonstrated NEGR1 known to regulate neurotransmission is detected in salivary gland and mediate muscarinic transcellular water movement. It is proven no change of morphology in *Negr1* knock-out mice. Lack of salivation is expected by decreased intracellular Ca^{2+} signaling and AQP5 translocation.

The result suggested that NEGR1 has a major role in intracellular Ca^{2+} signaling. In particular, it is a new finding that NEGR1 control SOCE. Therefore, it is curious to confirm whether NEGR1 regulates another receptor signaling. Additionally, it deserved that NEGR1 mediate GPCR-Ca^{2+} signaling in other tissue such as adipocyte.

NEGR1 as one of the immunoglobulin LON (IgLON) family has three Ig-like domains and localize in membrane rafts. Moreover, *Negr1* as a gene newly detected in obesity is revealed that association with human obesity (Kim, Chun et al. 2017, Flores-Dorantes, Diaz-Lopez et al. 2020). However, the molecular mechanism of obesity is not well known and the obesity of mice deleted gene is in conflict (Joo, Kim et al. 2019, Noh, Park et al. 2020). Compared to this, the neuronal function of NEGR1 is clear more. It demonstrated NEGR1 is a crucial factor in a transcriptome-wide association study of major depression (Dall'Aglio, Lewis et al. 2021). Especially, NEGR1 is associated with Alzheimer, schizophrenia, autism spectrum disorder (Noh, Park et al. 2020).

In a previous study, NEGR1 has two important neuronal phenotypes that NMDA-LTP reduction and synaptogenesis decline. NMDA receptor activity induced by high-frequency stimulation activates plasma membrane translocation of AMPA receptor, called long-term potentiation (LTP) and this reaction is reduced markedly

in *Negr1* KO mice (Noh, Lee et al. 2019). It is very similar to the role of NEGR1 in salivary gland. It detected reduction of muscarinic Ca^{2+} signaling and loss of aquaporin-5 translocation in *Negr1* KO mice. These results imply that NEGR1 commonly control in neuron and salivary gland cell that cytosolic Ca^{2+} signaling (i.e. NMDA receptor-mediated vs muscarinic receptor-mediated) induces receptor translocation to the membrane (i.e. AMPA receptor vs aquaporin-5). This provides a detailed understanding of the molecular mechanism of NEGR1 and the meaning of similarity in neuron and salivary gland cells simultaneously. It is expected that many neuro-exocrine common factors emerge newly and reveal their functions.

The contribution of salivary gland cells as well as neurons to salivation is important. Therefore, the decrease in salivation seen in *Negr1* KO mice also needs to be looked at in terms of salivary gland cells and neurons. In this study, we focused on NEGR1 in salivary gland cells. Neuronal NEGR1 contributes to salivation remains unknown. A Previous study found that the neurotransmitter release efficiency of excitatory synapse did not change in *Negr1* KO mice (Noh, Lee et al. 2019), and therefore the possibility was low that decreased salivary gland function results from the change of the neurotransmitter secretion efficiency. However, a decrease in miniature EPSC frequency was observed in *Negr1* KO mice, indicating a decrease in synaptogenesis (Noh, Lee et al. 2019). The function of NEGR1 to synaptogenesis is implemented in the salivary gland will be a very interesting topic.

In the co-culture of salivary glands and neurons, neurons self-organize around salivary epithelial cells (Sommakia and Baker 2016). In addition, the salivary glands secrete neurotrophins including brain-derived neurotrophic factor (BDNF),

thereby promoting neuron survival and differentiation and triggering synaptogenesis (Saruta, To et al. 2020). Therefore, it remains possible that the decrease in salivary secretion seen in *Negr1* KO mice is due to synaptogenesis that connects newly formed salivary gland cells and nerves. To date, the regulatory mechanism of synaptogenesis connecting salivary gland cells and nerves is not yet known in detail. Therefore, it will be a very interesting topic to examine whether this phenomenon actually occurs in the SMG and how this defect contributes to the hyposalivation of *Negr1* KO mice using *Negr1* conditional KO mice in the future.

Conclusion

Chapter 1. Ca^{2+}-activated chloride channels expression in mouse submandibular gland (SMG) cells

- *Anoctamins* were detected more expression in the acinar cells than the ductal cells of mouse SMG.
- Especially, *Ano1* is expressed in the only acinar cell of mouse SMG.
- Segment 'ac' form of *Ano1* is major splice variants in mouse SMG acinar cells.

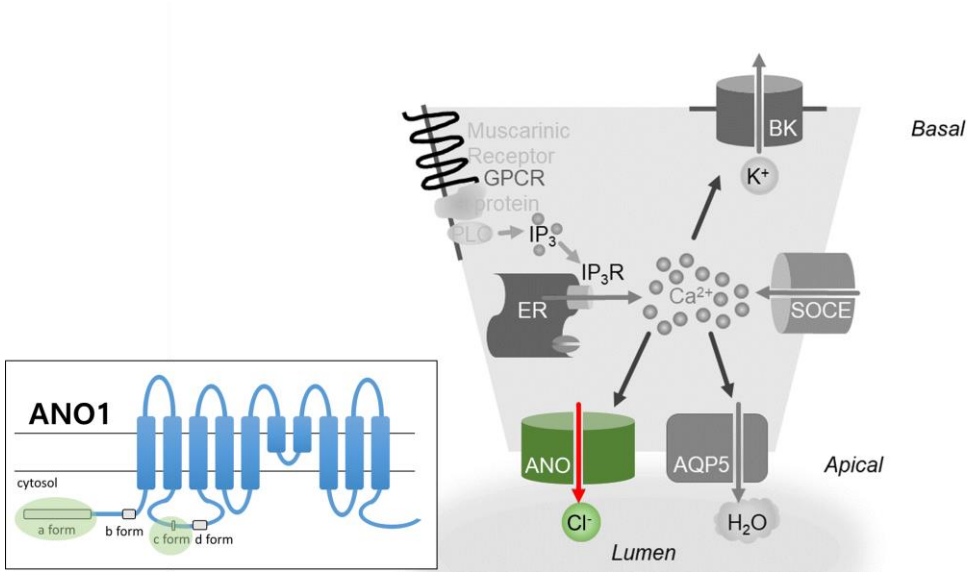

Chapter 2. The Effect of Ca^{2+} signal and Ca^{2+}-activated potassium channels on lipid raft microdomain in mouse SMG cells

- Methyl-β-cyclodextrin (MβCD) disrupts lipid raft microdomains by depleting cholesterol in salivary gland cells.
- MβCD preincubation inhibited muscarinic receptor-mediated Ca^{2+} signaling, but not inhibit a Ca^{2+} increase induced by thapsigargin, which activates store-operated Ca^{2+} entry (SOCE) in mouse SMG acinar cells.
- MβCD increased the activity of the Ca^{2+}-activated K^+ channel (BK channel) in mouse SMG acinar cells.
- MβCD did not directly affect the translocation of aquaporin-5 (AQP5) into the plasma membrane.

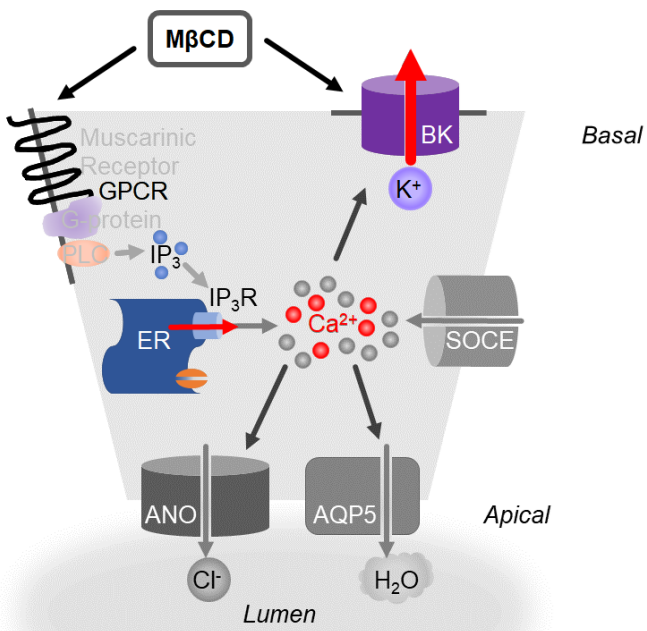

Chapter 3. The regulation of neuro-exocrine common factors on Ca^{2+} signal and Ca^{2+}-activated ion channels in mouse SMG cells

- *Negr1* is expressed in the SMG cells.
- Carbachol- or thapsigargin-induced intracellular Ca2+ increases were decreased in SMG cells of *Negr1* KO mice.
- BK channel activity is increased, but ANO1 channel currents are unchanged in *Negr1* KO mice.
- AQP5 translocation was reduced in *Negr1* KO mice.

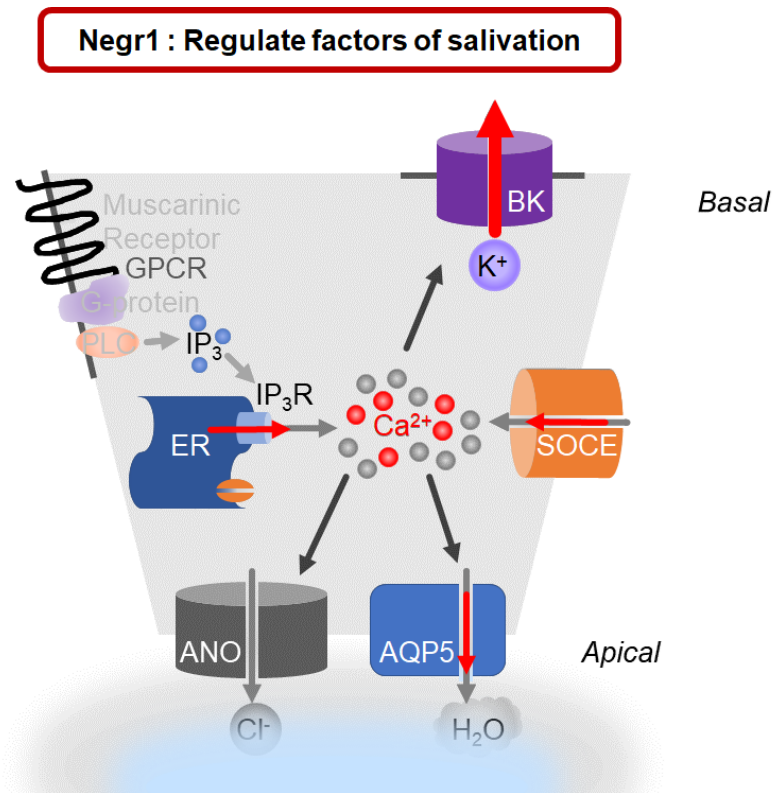

References

Allen, J. A., R. A. Halverson-Tamboli and M. M. Rasenick (2007). "Lipid raft microdomains and neurotransmitter signalling." Nat Rev Neurosci **8**(2): 128-140.

Ambudkar, I. S. (2014). "Ca(2)(+) signaling and regulation of fluid secretion in salivary gland acinar cells." Cell Calcium **55**(6): 297-305.

Ambudkar, I. S. (2016). "Calcium signalling in salivary gland physiology and dysfunction." J Physiol **594**(11): 2813-2824.

Ambudkar, I. S., L. B. de Souza and H. L. Ong (2017). "TRPC1, Orai1, and STIM1 in SOCE: Friends in tight spaces." Cell Calcium **63**: 33-39.

Asakura, K., A. Ueda, S. Shima, T. Ishikawa, C. Hikichi, S. Hirota, T. Fukui, S. Ito and T. Mutoh (2014). "Targeting of aquaporin 4 into lipid rafts and its biological significance." Brain Res **1583**: 237-244.

Aureli, M., S. Grassi, S. Prioni, S. Sonnino and A. Prinetti (2015). "Lipid membrane domains in the brain." Biochim Biophys Acta **1851**(8): 1006-1016.

Becchetti, A., L. Munaron and A. Arcangeli (2013). "The role of ion channels and transporters in cell proliferation and cancer." Front Physiol **4**: 312.

Benarroch, E. E. (2017). "Anoctamins (TMEM16 proteins): Functions and involvement in neurologic disease." Neurology **89**(7): 722-729.

Berg, J., H. Yang and L. Y. Jan (2012). "Ca2+-activated Cl- channels at a glance." J Cell Sci **125**(Pt 6): 1367-1371.

Bhattarai, K. R., R. Junjappa, M. Handigund, H. R. Kim and H. J. Chae (2018). "The imprint of salivary secretion in autoimmune disorders and related pathological conditions." Autoimmun Rev **17**(4): 376-390.

Bukiya, A. N., J. D. Belani, S. Rychnovsky and A. M. Dopico (2011). "Specificity of cholesterol and analogs to modulate BK channels points to direct sterol-channel protein interactions." J Gen Physiol **137**(1): 93-110.

Bukiya, A. N., T. Vaithianathan, G. Kuntamallappanavar, M. Asuncion-Chin and A. M. Dopico (2011). "Smooth muscle cholesterol enables BK beta1 subunit-mediated channel inhibition and subsequent vasoconstriction evoked by alcohol." Arterioscler Thromb Vasc Biol **31**(11): 2410-2423.

Caputo, A., E. Caci, L. Ferrera, N. Pedemonte, C. Barsanti, E. Sondo, U. Pfeffer, R. Ravazzolo, O. Zegarra-Moran and L. J. Galietta (2008). "TMEM16A, a membrane protein associated with calcium-dependent chloride channel activity." Science **322**(5901): 590-594.

Catalan, M. A., Y. Kondo, G. Pena-Munzenmayer, Y. Jaramillo, F. Liu, S. Choi, E. Crandall, Z. Borok, P. Flodby, G. E. Shull and J. E. Melvin (2015). "A fluid secretion

pathway unmasked by acinar-specific Tmem16A gene ablation in the adult mouse salivary gland." Proc Natl Acad Sci U S A **112**(7): 2263-2268.

Catalan, M. A., T. Nakamoto and J. E. Melvin (2009). "The salivary gland fluid secretion mechanism." J Med Invest **56 Suppl**: 192-196.

Concepcion, A. R. and S. Feske (2017). "Regulation of epithelial ion transport in exocrine glands by store-operated Ca(2+) entry." Cell Calcium **63**: 53-59.

Dall'Aglio, L., C. M. Lewis and O. Pain (2021). "Delineating the Genetic Component of Gene Expression in Major Depression." Biol Psychiatry **89**(6): 627-636.

Delporte, C. (2014). "Aquaporins in salivary glands and pancreas." Biochim Biophys Acta **1840**(5): 1524-1532.

Dionisio, N., C. Galan, I. Jardin, G. M. Salido and J. A. Rosado (2011). "Lipid rafts are essential for the regulation of SOCE by plasma membrane resident STIM1 in human platelets." Biochim Biophys Acta **1813**(3): 431-437.

Dopico, A. M., A. N. Bukiya and A. K. Singh (2012). "Large conductance, calcium- and voltage-gated potassium (BK) channels: regulation by cholesterol." Pharmacol Ther **135**(2): 133-150.

Duran, C. and H. C. Hartzell (2011). "Physiological roles and diseases of Tmem16/Anoctamin proteins: are they all chloride channels?" Acta Pharmacol Sin **32**(6): 685-692.

Ferrera, L., A. Caputo and L. J. Galietta (2010). "TMEM16A protein: a new identity for Ca(2+)-dependent Cl(-) channels." Physiology (Bethesda) **25**(6): 357-363.

Ferrera, L., A. Caputo, I. Ubby, E. Bussani, O. Zegarra-Moran, R. Ravazzolo, F. Pagani and L. J. Galietta (2009). "Regulation of TMEM16A chloride channel properties by alternative splicing." J Biol Chem **284**(48): 33360-33368.

Flores-Dorantes, M. T., Y. E. Diaz-Lopez and R. Gutierrez-Aguilar (2020). "Environment and Gene Association With Obesity and Their Impact on Neurodegenerative and Neurodevelopmental Diseases." Front Neurosci **14**: 863.

Galan, C., G. E. Woodard, N. Dionisio, G. M. Salido and J. A. Rosado (2010). "Lipid rafts modulate the activation but not the maintenance of store-operated Ca(2+) entry." Biochim Biophys Acta **1803**(9): 1083-1093.

Gao, X., M. S. Oei, C. E. Ovitt, M. Sincan and J. E. Melvin (2018). "Transcriptional profiling reveals gland-specific differential expression in the three major salivary glands of the adult mouse." Physiol Genomics **50**(4): 263-271.

Gluck, C., S. Min, A. Oyelakin, K. Smalley, S. Sinha and R. A. Romano (2016). "RNA-seq based transcriptomic map reveals new insights into mouse salivary gland development

and maturation." BMC Genomics **17**(1): 923.

Gueguinou, M., A. Gambade, R. Felix, A. Chantome, Y. Fourbon, P. Bougnoux, G. Weber, M. Potier-Cartereau and C. Vandier (2015). "Lipid rafts, KCa/ClCa/Ca2+ channel complexes and EGFR signaling: Novel targets to reduce tumor development by lipids?" Biochim Biophys Acta **1848**(10 Pt B): 2603-2620.

Habbab, K. M., D. R. Moles and S. R. Porter (2010). "Potential oral manifestations of cardiovascular drugs." Oral Dis **16**(8): 769-773.

Han, J. H., H. M. Kim, D. G. Seo, G. Lee, E. B. Jeung and F. H. Yu (2015). "Multiple transcripts of anoctamin genes expressed in the mouse submandibular salivary gland." J Periodontal Implant Sci **45**(2): 69-75.

Ishikawa, Y., G. Cho, Z. Yuan, N. Inoue and Y. Nakae (2006). "Aquaporin-5 water channel in lipid rafts of rat parotid glands." Biochim Biophys Acta **1758**(8): 1053-1060.

Jardin, I., G. M. Salido and J. A. Rosado (2008). "Role of lipid rafts in the interaction between hTRPC1, Orai1 and STIM1." Channels (Austin) **2**(6): 401-403.

Jensen, S. B. and A. Vissink (2014). "Salivary gland dysfunction and xerostomia in Sjogren's syndrome." Oral Maxillofac Surg Clin North Am **26**(1): 35-53.

Jin, M., S. M. Hwang, A. J. Davies, Y. Shin, J. S. Bae, J. H. Lee, E. B. Lee, Y. W. Song and K. Park (2012). "Autoantibodies in primary Sjogren's syndrome patients induce internalization of muscarinic type 3 receptors." Biochim Biophys Acta **1822**(2): 161-167.

Joo, Y., H. Kim, S. Lee and S. Lee (2019). "Neuronal growth regulator 1-deficient mice show increased adiposity and decreased muscle mass." Int J Obes (Lond) **43**(9): 1769-1782.

Kann, O., N. Taubenberger, C. Huchzermeyer, I. E. Papageorgiou, F. Benninger, U. Heinemann and R. Kovacs (2012). "Muscarinic receptor activation determines the effects of store-operated Ca(2+)-entry on excitability and energy metabolism in pyramidal neurons." Cell Calcium **51**(1): 40-50.

Kim, H., Y. Chun, L. Che, J. Kim, S. Lee and S. Lee (2017). "The new obesity-associated protein, neuronal growth regulator 1 (NEGR1), is implicated in Niemann-Pick disease Type C (NPC2)-mediated cholesterol trafficking." Biochem Biophys Res Commun **482**(4): 1367-1374.

Kim, J. H., S. H. Park, Y. W. Moon, S. Hwang, D. Kim, S. H. Jo, S. B. Oh, J. S. Kim, J. W. Jahng, J. H. Lee, S. J. Lee, S. Y. Choi and K. Park (2009). "Histamine H1 receptor induces cytosolic calcium increase and aquaporin translocation in human salivary gland cells." J Pharmacol Exp Ther **330**(2): 403-412.

Koudinov, A. R. and N. V. Koudinova (2001). "Essential role for cholesterol in synaptic plasticity and neuronal degeneration." FASEB J **15**(10): 1858-1860.

Lee, B. H., A. E. Gauna, G. Perez, Y. J. Park, K. M. Pauley, T. Kawai and S. Cha (2013). "Autoantibodies against muscarinic type 3 receptor in Sjogren's syndrome inhibit aquaporin 5 trafficking." PLoS One **8**(1): e53113.

Lee, B. M., H. Jo, G. Park, Y. H. Kim, C. K. Park, S. J. Jung, G. Chung and S. B. Oh (2017). "Extracellular ATP Induces Calcium Signaling in Odontoblasts." J Dent Res **96**(2): 200-207.

Lee, J., Y. J. Kim, L. M. Choi, K. Lee, H. K. Park and S. Y. Choi (2021). "Muscarinic Receptors and BK Channels Are Affected by Lipid Raft Disruption of Salivary Gland Cells." Int J Mol Sci **22**(9).

Lee, K., Y. J. Kim, L. M. Choi, S. Choi, H. Nam, H. Y. Ko, G. Chung, J. H. Lee, S. H. Jo, G. Lee, S. Y. Choi and K. Park (2017). "Human salivary gland cells express bradykinin receptors that modulate the expression of proinflammatory cytokines." Eur J Oral Sci **125**(1): 18-27.

Lippiat, J. D., N. B. Standen, I. D. Harrow, S. C. Phillips and N. W. Davies (2003). "Properties of BK(Ca) channels formed by bicistronic expression of hSloalpha and beta1-4 subunits in HEK293 cells." J Membr Biol **192**(2): 141-148.

Maccarrone, G., C. Ditzen, A. Yassouridis, C. Rewerts, M. Uhr, M. Uhlen, F. Holsboer and C. W. Turck (2013). "Psychiatric patient stratification using biosignatures based on cerebrospinal fluid protein expression clusters." J Psychiatr Res **47**(11): 1572-1580.

Melvin, J. E. (1999). "Chloride channels and salivary gland function." Crit Rev Oral Biol Med **10**(2): 199-209.

Miyata, S., N. Matsumoto, K. Taguchi, A. Akagi, T. Iino, N. Funatsu and S. Maekawa (2003). "Biochemical and ultrastructural analyses of IgLON cell adhesion molecules, Kilon and OBCAM in the rat brain." Neuroscience **117**(3): 645-658.

Modeer, T., C. C. Blomberg, B. Wondimu, A. Julihn and C. Marcus (2010). "Association between obesity, flow rate of whole saliva, and dental caries in adolescents." Obesity (Silver Spring) **18**(12): 2367-2373.

Nakamoto, T., V. G. Romanenko, A. Takahashi, T. Begenisich and J. E. Melvin (2008). "Apical maxi-K (KCa1.1) channels mediate K+ secretion by the mouse submandibular exocrine gland." Am J Physiol Cell Physiol **294**(3): C810-819.

Ngamchuea, K., K. Chaisiwamongkhol, C. Batchelor-McAuley and R. G. Compton (2018). "Correction: Chemical analysis in saliva and the search for salivary biomarkers - a tutorial review." Analyst **143**(3): 777-783.

Noh, K., H. Lee, T. Y. Choi, Y. Joo, S. J. Kim, H. Kim, J. Y. Kim, J. W. Jahng, S. Lee, S. Y. Choi and S. J. Lee (2019). "Negr1 controls adult hippocampal neurogenesis and affective

behaviors." Mol Psychiatry **24**(8): 1189-1205.

Noh, K., J. C. Park, J. S. Han and S. J. Lee (2020). "From Bound Cells Comes a Sound Mind: The Role of Neuronal Growth Regulator 1 in Psychiatric Disorders." Exp Neurobiol **29**(1): 1-10.

Oldfield, S., J. Hancock, A. Mason, S. A. Hobson, D. Wynick, E. Kelly, A. D. Randall and N. V. Marrion (2009). "Receptor-mediated suppression of potassium currents requires colocalization within lipid rafts." Mol Pharmacol **76**(6): 1279-1289.

Oyelakin, A., E. A. C. Song, S. Min, J. E. Bard, J. V. Kann, E. Horeth, K. Smalley, J. M. Kramer, S. Sinha and R. A. Romano (2019). "Transcriptomic and Single-Cell Analysis of the Murine Parotid Gland." J Dent Res **98**(13): 1539-1547.

Pani, B., X. Liu, S. Bollimuntha, K. T. Cheng, I. R. Niesman, C. Zheng, V. R. Achen, H. H. Patel, I. S. Ambudkar and B. B. Singh (2013). "Impairment of TRPC1-STIM1 channel assembly and AQP5 translocation compromise agonist-stimulated fluid secretion in mice lacking caveolin1." J Cell Sci **126**(Pt 2): 667-675.

Pedemonte, N. and L. J. Galietta (2014). "Structure and function of TMEM16 proteins (anoctamins)." Physiol Rev **94**(2): 419-459.

Pedersen, A. M. L., C. E. Sorensen, G. B. Proctor, G. H. Carpenter and J. Ekstrom (2018). "Salivary secretion in health and disease." J Oral Rehabil **45**(9): 730-746.

Proctor, G. B. (2016). "The physiology of salivary secretion." Periodontol 2000 **70**(1): 11-25.

Proctor, G. B. and G. H. Carpenter (2007). "Regulation of salivary gland function by autonomic nerves." Auton Neurosci **133**(1): 3-18.

Riddle, M. A., J. M. Hughes and B. R. Walker (2011). "Role of caveolin-1 in endothelial BKCa channel regulation of vasoreactivity." Am J Physiol Cell Physiol **301**(6): C1404-1414.

Romanenko, V. G., M. A. Catalan, D. A. Brown, I. Putzier, H. C. Hartzell, A. D. Marmorstein, M. Gonzalez-Begne, J. R. Rock, B. D. Harfe and J. E. Melvin (2010). "Tmem16A encodes the Ca2+-activated Cl- channel in mouse submandibular salivary gland acinar cells." J Biol Chem **285**(17): 12990-13001.

Romanenko, V. G., T. Nakamoto, A. Srivastava, T. Begenisich and J. E. Melvin (2007). "Regulation of membrane potential and fluid secretion by Ca2+-activated K+ channels in mouse submandibular glands." J Physiol **581**(Pt 2): 801-817.

Romanenko, V. G., J. Thompson and T. Begenisich (2010). "Ca2+-activated K channels in parotid acinar cells: The functional basis for the hyperpolarized activation of BK channels." Channels (Austin) **4**(4): 278-288.

Roussa, E. (2011). "Channels and transporters in salivary glands." Cell Tissue Res **343**(2): 263-287.

Saitou, M., E. A. Gaylord, E. Xu, A. J. May, L. Neznanova, S. Nathan, A. Grawe, J. Chang, W. Ryan, S. Ruhl, S. M. Knox and O. Gokcumen (2020). "Functional Specialization of Human Salivary Glands and Origins of Proteins Intrinsic to Human Saliva." Cell Rep **33**(7): 108402.

Saruta, J., M. To, W. Sakaguchi, Y. Kondo and K. Tsukinoki (2020). "Brain-derived neurotrophic factor is related to stress and chewing in saliva and salivary glands." Jpn Dent Sci Rev **56**(1): 43-49.

Schroeder, B. C., T. Cheng, Y. N. Jan and L. Y. Jan (2008). "Expression cloning of TMEM16A as a calcium-activated chloride channel subunit." Cell **134**(6): 1019-1029.

Sebastiao, A. M., M. Colino-Oliveira, N. Assaife-Lopes, R. B. Dias and J. A. Ribeiro (2013). "Lipid rafts, synaptic transmission and plasticity: impact in age-related neurodegenerative diseases." Neuropharmacology **64**: 97-107.

Sekiguchi, R., D. Martin, Genomics, C. Computational Biology and K. M. Yamada (2020). "Single-Cell RNA-seq Identifies Cell Diversity in Embryonic Salivary Glands." J Dent Res **99**(1): 69-78.

Simons, K. and J. L. Sampaio (2011). "Membrane organization and lipid rafts." Cold Spring Harb Perspect Biol **3**(10): a004697.

Sirtori, C. R. (2014). "The pharmacology of statins." Pharmacol Res **88**: 3-11.

Sommakia, S. and O. J. Baker (2016). "Neurons Self-Organize Around Salivary Epithelial Cells in Novel Co-Culture Model." J Stem Cell Regen Biol **2**(2).

Song, E. C., S. Min, A. Oyelakin, K. Smalley, J. E. Bard, L. Liao, J. Xu and R. A. Romano (2018). "Genetic and scRNA-seq Analysis Reveals Distinct Cell Populations that Contribute to Salivary Gland Development and Maintenance." Sci Rep **8**(1): 14043.

Strege, P. R., S. J. Gibbons, A. Mazzone, C. E. Bernard, A. Beyder and G. Farrugia (2017). "EAVK segment "c" sequence confers Ca(2+)-dependent changes to the kinetics of full-length human Ano1." Am J Physiol Gastrointest Liver Physiol **312**(6): G572-G579.

Stummann, T. C., J. H. Poulsen, A. Hay-Schmidt, M. Grunnet, D. A. Klaerke, H. B. Rasmussen, S. P. Olesen and N. K. Jorgensen (2003). "Pharmacological investigation of the role of ion channels in salivary secretion." Pflugers Arch **446**(1): 78-87.

Sung, T. S., K. O'Driscoll, H. Zheng, N. J. Yapp, N. Leblanc, S. D. Koh and K. M. Sanders (2016). "Influence of intracellular Ca2+ and alternative splicing on the pharmacological profile of ANO1 channels." Am J Physiol Cell Physiol **311**(3): C437-451.

Tada, J., T. Sawa, N. Yamanaka, M. Shono, T. Akamatsu, K. Tsumura, M. N. Parvin, N.

Kanamori and K. Hosoi (1999). "Involvement of vesicle-cytoskeleton interaction in AQP5 trafficking in AQP5-gene-transfected HSG cells." Biochem Biophys Res Commun **266**(2): 443-447.

Tajima, N., Y. Itokazu, E. R. Korpi, P. Somerharju and R. Kakela (2011). "Activity of BK(Ca) channel is modulated by membrane cholesterol content and association with Na+/K+-ATPase in human melanoma IGR39 cells." J Biol Chem **286**(7): 5624-5638.

Tamasi, V., P. Petschner, C. Adori, E. Kirilly, R. D. Ando, L. Tothfalusi, G. Juhasz and G. Bagdy (2014). "Transcriptional evidence for the role of chronic venlafaxine treatment in neurotrophic signaling and neuroplasticity including also Glutamatergic [corrected] - and insulin-mediated neuronal processes." PLoS One **9**(11): e113662.

Villar, V. A., S. Cuevas, X. Zheng and P. A. Jose (2016). "Localization and signaling of GPCRs in lipid rafts." Methods Cell Biol **132**: 3-23.

Wang, C. S., Y. Wee, C. H. Yang, J. E. Melvin and O. J. Baker (2016). "ALX/FPR2 Modulates Anti-Inflammatory Responses in Mouse Submandibular Gland." Sci Rep **6**: 24244.

Weaver, A. K., M. L. Olsen, M. B. McFerrin and H. Sontheimer (2007). "BK channels are linked to inositol 1,4,5-triphosphate receptors via lipid rafts: a novel mechanism for coupling [Ca(2+)](i) to ion channel activation." J Biol Chem **282**(43): 31558-31568.

Yang, H., G. Zhang and J. Cui (2015). "BK channels: multiple sensors, one activation gate." Front Physiol **6**: 29.

Yang, Y. D., H. Cho, J. Y. Koo, M. H. Tak, Y. Cho, W. S. Shim, S. P. Park, J. Lee, B. Lee, B. M. Kim, R. Raouf, Y. K. Shin and U. Oh (2008). "TMEM16A confers receptor-activated calcium-dependent chloride conductance." Nature **455**(7217): 1210-1215.

국문초록

타액선에서 칼슘 신호와 이온 채널의 조절

이 지 수

서울대학교 대학원 치의생명과학과 치의생명과학전공

(지도교수: 최 세 영)

인간은 하루에 최소 0.5L에서 최대 2L까지 타액을 생성한다. 타액 분비가 과다하거나 부족하면 일상 생활의 큰 불편을 초래한다. 타액을 분비하는 주요 타액선(salivary gland)의 종류는 크게 세 부분으로 나뉘는데, 귀밑샘(parotid gland), 턱밑샘(submandibular gland), 혀밑샘(subligual gland)이다. 특정 자극이 없을 때, 이 중의 턱밑샘에서 침의 3분의 2가 생성된다. 또한 타액선을 구성하는 세포를 크게 두 부류로 나눌 수 있는데, 선포 세포(acinar cell)에서 타액을 생성하고 이는 췌관 세포(dutcal cell)을 통하여 이동하여 분비된다. 타액은 여러 이온(ion)들이 녹아져 있는 유동체(fluid) 형태의 혼합물이다. 이를 생성하고 분비하는 데에 수많은 이온 수송체(ion transporter)들이 관여한다. 이러한 이온 수송체들이 활성화되기 위해서 세포 내 칼슘

농도의 변화가 신호로 작용한다. 타액선의 세포에서 발현이 예상되는 칼슘을 매개로 활성화되는 이온 채널(ion channel)들이 있지만, 정확한 종류와 기전은 아직도 모르는 부분이 많다. 이 연구에서는 생쥐의 턱밑샘에서 칼슘 신호에 의해 활성화되는 이온 채널의 종류를 규명하고, 기능의 차이를 비교하여 타액 분비에 미치는 영향을 규명하고자 한다.

타액이 생성되기 위해 세포 안과 밖의 삼투압 차이를 유발하는 칼슘 의존성 염소 채널의 종류를 확인하고자 선포 세포와 췌관 세포를 구별하여 유전자 발현을 비교하였다. 하나의 턱밑샘 세포에 여러 종류의 칼슘 의존성 염소 채널이 존재하였고, 그 중 Anoctamin1은 선포세포에서만 발현함을 확인하였다.

또한, 세포 내 신호전달을 조절하는 중요한 역할을 할 것이라고 알려진 세포막의 지질 다량 미세 영역 (lipid raft microdomain)이 타액선의 미치는 영향을 보고자, 이를 없애 생쥐 턱밑샘 세포에서 생리적 기능의 변화를 확인하였다. 이 부분이 망가져도 세포의 생존에는 큰 차이를 보이지 않았지만, GPCR cascade를 통한 세포 내의 칼슘 신호가 줄었고 칼슘 의존성 포타슘 채널의 활성은 증가하였다.

마지막으로, 신경세포에서 분비를 조절하는 인자가 타액선에서도 분비 조절인자로 작용할 수 있는지 확인하는 실험을 진행하였다. 타액분비 조절인자의 후보군인 유전자(neuronal growth regulator-1)가 결손된 생쥐를 이용하여 확인하였을 때, 세포 내의 칼슘 변화가 감소했고 칼슘 의존성 포타슘 채널의 활성은 증가하였지만 칼슘 의존성 염소 채널의 활성은 차이가 없었으며 물 이온 통로의 발현이 감소하였다.

이러한 연구들을 통해 타액선 세포에서의 칼슘 의존성 이온 채널들의 발현과 기능의 변화를 규명하여 타액의 분비 원리를 더욱 명확하게

이해할 수 있었다. 이를 확장하여 타액선의 큰 질병인 구강건조증의 효과적인 치료를 위한 표적이 될 수 있을 것으로 기대된다.

주요어 : 타액선, 이온 채널, 칼슘 이온, Lipid raft microdomain.
학 번 : 2013-23556